Chemical Science

ROYAL SOCIETY OF CHEMISTRY

REVIEW

View Article Online
View Journal | View Issue

Check for updates

Cite this: *Chem. Sci.*, 2022, **13**, 3625

Recent progress in thermally activated delayed fluorescence emitters for nondoped organic light-emitting diodes

Yi-Zhong Shi, † Hao Wu,† Kai Wang, * Jia Yu, Xue-Mei Ou and Xiao-Hong Zhang *

Received 24th December 2021
Accepted 21st February 2022

DOI: 10.1039/d1sc07180g

rsc.li/chemical-science

Nondoped organic light-emitting diodes (OLEDs) have drawn immense attention due to their merits of process simplicity, reduced fabrication cost, *etc.* To realize high-performance nondoped OLEDs, all electrogenerated excitons should be fully utilized. The thermally activated delayed fluorescence (TADF) mechanism can theoretically realize 100% internal quantum efficiency (IQE) through an effective upconversion process from nonradiative triplet excitons to radiative singlet ones. Nevertheless, exciton quenching, especially related to triplet excitons, is generally very serious in TADF-based nondoped OLEDs, significantly hindering the pace of development. Enormous efforts have been devoted to alleviating the annoying exciton quenching process, and a number of TADF materials for highly efficient nondoped devices have been reported. In this review, we mainly discuss the mechanism, exciton leaking channels, and reported molecular design strategies of TADF emitters for nondoped devices. We further classify their molecular structures depending on the functional A groups and offer an outlook on their future prospects. It is anticipated that this review can entice researchers to recognize the importance of TADF-based nondoped OLEDs and provide a possible guide for their future development.

Open Access Article. Published on 22 febbraio 2022. Downloaded on 08/05/2026 07:17:27.
This article is licensed under a Creative Commons Attribution-NonCommercial 3.0 Unported Licence.

1. Introduction

Organic light-emitting diode (OLED) technology has been extensively applied in high-end solid-state lighting and flat-panel displays owing to its superior advantages of autoluminescence, low driving voltage, flexibility, fast response, and so on.[1] According to the spin statistics, electrogenerated singlet and triplet excitons have a ratio of 1 : 3. Traditional fluorescent materials with high photoluminescence quantum yields (PLQYs) can only utilize singlet excitons, while the energies of triplet excitons are depleted *via* nonradiative transition processes. To realize full exciton utilization, phosphorescence and thermally activated delayed fluorescence (TADF) emitters have been proposed.[2,3] Phosphorescence emitters can utilize triplet excitons due to the strong spin–orbit coupling (SOC) induced by heavy atoms (*e.g.*, platinum and iridium), which can help to enhance the triplet radiation (*i.e.*, phosphorescence) rate. Although phosphorescence-based OLEDs are now the main commercial OLED technologies, they have several obvious drawbacks, such as high costs and toxicity due to heavy atoms and the absence of stable blue phosphorescence emitters. TADF-based OLEDs are an alternative approach with potential 100% internal quantum efficiencies (IQEs) and have attracted considerable attention within the last decade.[4–6]

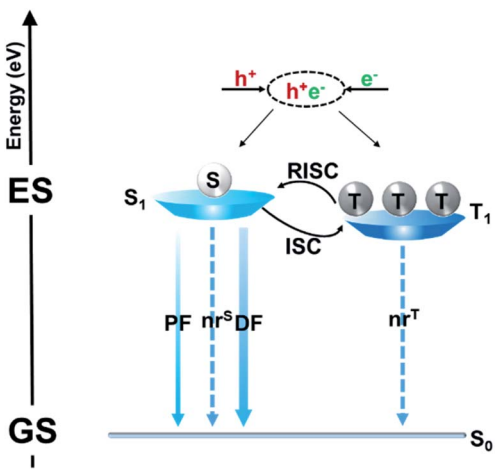

Fig. 1 Illustration of the exciton utilization channels of the TADF mechanism upon electrical excitation. GS and ES are ground and excited states, respectively; S and T are the electrogenerated singlet and triplet excitons; ISC and RISC are the intersystem crossing and reverse intersystem crossing processes; nr^S and nr^T are the non-radiative transition processes of the singlet and triplet excitons; PF and DF are the prompt and delayed fluorescence.

Institute of Functional Nano & Soft Materials (FUNSOM), Jiangsu Key Laboratory for Carbon-Based Functional Materials & Devices, Soochow University, 199 Ren'ai Road, Suzhou, Jiangsu, 215123, PR China. E-mail: xiaohong_zhang@suda.edu.cn; wkai@suda.edu.cn

† These authors contributed equally to this work.

© 2022 The Author(s). Published by the Royal Society of Chemistry

Open Access Article. Published on 22 febbraio 2022. Downloaded on 08/05/2026 07:17:27.
This article is licensed under a Creative Commons Attribution-NonCommercial 3.0 Unported Licence.

Fig. 1 illustrates a schematic illustration of exciton energy transfer and utilization in a TADF emitter upon electrical excitation. Singlet excitons have three possible energy decay routes: fluorescence radiation, nonradiative transition to the ground state (S_0) and intersystem crossing (ISC) from the lowest singlet excited state (S_1) to the lowest triplet excited state (T_1), while triplet excitons can either be upconverted into singlets *via* reverse intersystem crossing (RISC) or suffer nonradiative decay (assuming that the phosphorescence process can be ignored in conventional pure organic systems). RISC and fluorescence radiation are the key steps for triplet and singlet exciton harvesting, respectively. To realize a competitive RISC rate (k_{RISC}) to that of the corresponding triplet nonradiative process (k_{nr}^{T}), a small S_1–T_1 energy splitting (ΔE_{ST}) is required. To date, several design strategies have been proposed, such as highly twisted D–A molecular structures,[7–10] exciplex systems,[11–17] and the recently developed multiple resonance (MR) effect-induced TADF.[18–20] A common characteristic of these molecular designs is that they can all restrain the overlaps between the highest occupied molecular orbitals (HOMOs) and lowest unoccupied molecular orbitals (LUMOs), which is essential for small ΔE_{ST}s. Singlet–triplet spin–orbit coupling (SOC) is another factor that significantly affects the RISC process. It can be efficiently enhanced *via* either internal/external heavy atom effects[21–24] or excited states with a different nature.[25–28] Fluorescence radiation is the ultimate pathway for not only the initial singlet exciton harvest (prompt fluorescence, PF) but also the triplet exciton harvest *via* delayed fluorescence (DF). Thus, enhancing its rate (k_r) is also required to sufficiently surpass the singlet nonradiative decay rate (k_{nr}^{S}). While unlike small ΔE_{ST}s, which require the separation of frontier molecular orbitals (FMOs), a high k_r requires a sufficient integral between the HOMO and LUMO wavefunctions. Thus, how to strike a balance between small ΔE_{ST}s and fast k_r becomes key to obtaining optimized performances. PLQY is a parameter that contains both a prompt component that is directly related to the fluorescence process and a delayed component that is related to both the RISC and fluorescence processes. Thus, the PLQY reflects the overall exciton utilization and is typically positively correlated with the corresponding electroluminescent (EL) properties. A high PLQY is a prerequisite for a TADF emitter to realize high performances in OLEDs.

After the rapid development of the past dozen years, considerable progress has been made in developing high-performance TADF-OLEDs, and the reported maximum external quantum efficiencies (EQEs) have been beyond 30%.[29–39] In these OLEDs, emitting layers (EMLs) are all obtained by adopting optimized host–dopant configurations. This is mainly to suppress the annoying concentration quenching, especially arising from the long-lived triplet excitons. On the other hand, introducing host matrixes not only complicates device fabrication but also increases the cost of production.[40] For mass production, OLEDs with nondoped EMLs would be simpler and more attractive.

In this review, we first summarize the recent progress in the field of TADF emitters toward high-performance nondoped OLEDs, especially the important progress within the last two years. Then, we categorize the TADF emitters according to their different electron-withdrawing units and devote particular emphasis to molecular design strategies, which has not been done in previous reviews. In addition, their physical properties, as well as nondoped device performances, are also summarized. We further discuss the present pros and cons of TADF-based nondoped OLEDs and provide an outlook on their prospects.

2. Molecular design strategies of TADF emitters for nondoped OLEDs

To exploit novel TADF materials toward high-performance nondoped OLEDs, the abovementioned keys of general TADF molecular designs are still essential. In addition, energy loss channels in nondoped EMLs are more complicated than ideal host–guest EMLs and should be carefully blocked. In earlier studies, researchers have recognized that methods of rigidifying organic luminogens through viscous or solid environments or forming J-aggregates can give rise to emission enhancement.[41,42] In 2001, Tang *et al.* accidentally discovered enhanced emission upon aggregation for hexaphenylsilole (HPS) and named the phenomenon "aggregation-induced emission (AIE)".[43,44] Since then, AIE has been widely applied in the fields of optical devices, luminescent sensors, bioimaging, phototherapy, *etc.* Both theoretical simulation and experimental results suggest that in their aggregate states, molecular vibrations and rotations are evidently suppressed, resulting in decreased k_{nr}^{S} and thus enhanced emission. In particular, some emitters exhibit aggregation-induced delayed fluorescence (AIDF) behaviors (as shown in Fig. 2a).[45] Emitters with such AIE/AIDF behaviors are promising candidates for high-efficiency nondoped OLEDs. Many AIE-TADF/AIDF emitters have been reported to show decent performances in nondoped OLEDs.

In nondoped OLEDs, intermolecular exciton quenching plays a vital role in causing exciton loss. Many studies have suggested that suppressing the annihilation process associated with long-lived triplet states is key to determining nondoped device performance. The rate constant of triplet-related quenching (k_{CQ}) can be expressed as follows:

$$k_{CQ}(R) = k_{RISC} \exp\left\{\frac{2R_0}{L_{ET}}\left(1 - \frac{R}{R_0}\right)\right\} \quad (1)$$

where R_0 is the critical intermolecular distance at which concentration quenching and RISC occurred with the same probability, and L_{ET} is the effective electron tunneling distance, which quantifies the intermolecular electron-exchange interactions. According to eqn (1), k_{CQ} exhibits an exponential dependence on the average intermolecular distance (R) in the thin films, which agrees well with the Dexter energy-transfer model, and thus, short-range electron-exchange interactions should be well blocked. Therefore, isolating triplet excitons in amorphous neat films is key to suppressing their related quenching and realizing high-performance nondoped OLED performances. Introducing steric hindrance of TADF emitters is one of the most feasible methods to enlarge the intermolecular distance. Fig. 2b displays a typical intermolecular interaction of such molecules.

© 2022 The Author(s). Published by the Royal Society of Chemistry

Open Access Article. Published on 22 febbraio 2022. Downloaded on 08/05/2026 07:17:27.
This article is licensed under a Creative Commons Attribution-NonCommercial 3.0 Unported Licence.

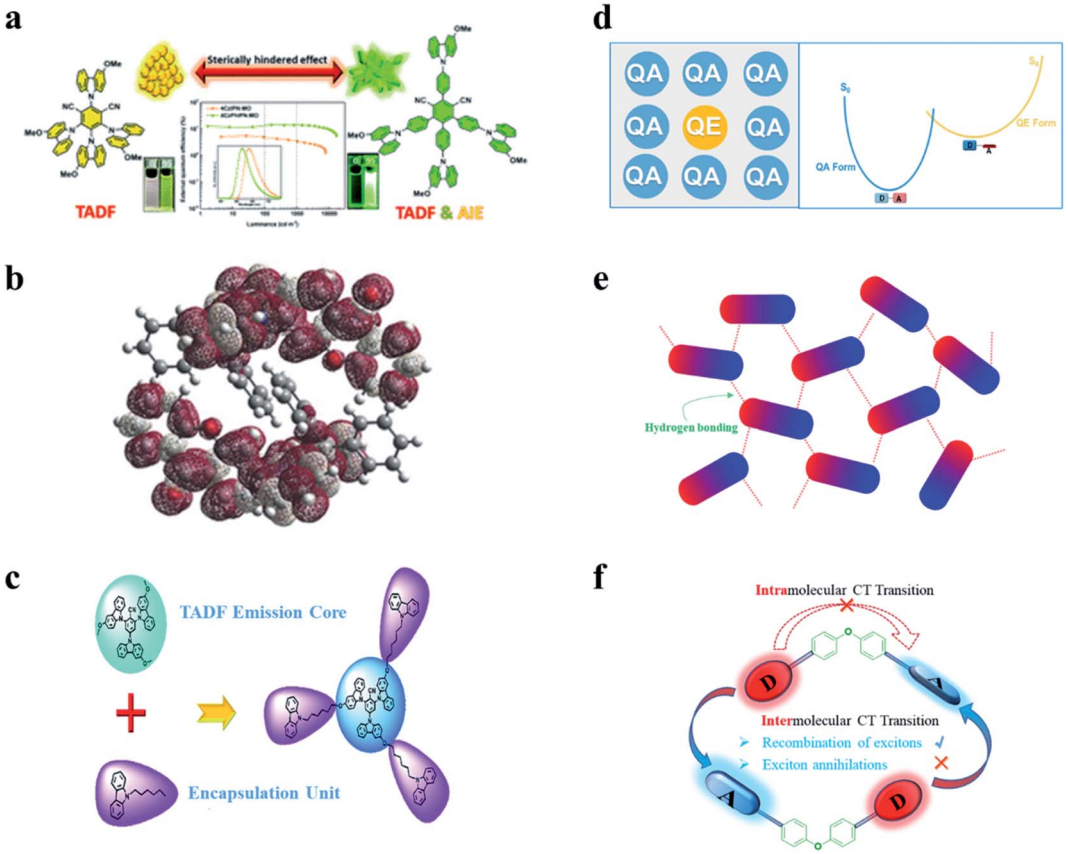

Fig. 2 Molecular design strategies of TADF emitters for nondoped OLEDs. (a) The AIE/AIDF mechanism. Reproduced from ref. 45 with permission. Copyright 2020 Wiley-VCH. (b) The mechanism of introducing steric hindrance. Reproduced from ref. 46 with permission. Copyright 2017 Wiley-VCH. (c) Self-host mechanism. Reproduced from ref. 47 with permission. Copyright 2019 the Royal Society of Chemistry. (d) The "self-doping" mechanism. Reproduced from ref. 49 with permission. Copyright 2021 Wiley-VCH. (e) Intermolecular hydrogen bonding mechanism. Reproduced from ref. 50 with permission. Copyright 2019 the Royal Society of Chemistry. (f) D–spacer–A mechanism. Reproduced from ref. 51 with permission. Copyright 2018 Wiley-VCH.

Theoretical calculations indicate that triplet spin-density distributions (SDDs) are centralized on the main body of the TADF emitters, while the phenyl moieties act as steric hindrances to realize loosely aligned molecules.[46] Distances between triplet excitons can be evidently enhanced in such molecular packings, and thus, it is expected that triplet exciton collision-induced concentration quenching can be well restrained.

In addition to introducing extra steric groups, integrating the host matrix and guest TADF emitters into new "self-host" materials is also a wise molecular design method for nondoped OLEDs. As displayed in Fig. 2c, introducing carbazoles as steric shields can not only keep the intrinsic TADF feature unchanged but also effectively suppress the exciton quenching caused by intermolecular interactions. Moreover, such "emission-core and host-encapsulation" molecular structures generally meet the requirements of the solution process and are thus usually applied in solution-processed nondoped OLEDs.[47,48]

It was recently recognized that some organic emitters actually have dual stable conformations. TADF is associated with the highly twisted conformation, which is also known as the "quasi-equatorial (QE)" conformation. On the other hand, the other mildly twisted form, referred to as the "quasi-axial (QA)" conformation, often shows only conventional fluorescence with higher energy instead of TADF. As displayed in Fig. 2d, by using the different characteristics of these conformers, our group proposed a new concept of "self-doping" for realizing high-efficiency nondoped OLEDs.[49] Interestingly, this "compositionally" pure film actually behaves as a film with a dopant (QE form) in a matrix (QA form). The concentration-induced quenching that may seriously occur at high concentrations is thus expected to be effectively relieved.

Hydrogen bonds, especially intermolecular bonds, have been widely used to construct rigid intermolecular frameworks to relieve molecular vibrational and rotational motions. Enormous highly efficient chromophores have been exploited based on hydrogen bonds. On this basis, we further proposed that in neat films of TADF emitters with suitable intermolecular hydrogen bonds, continuous and oriented interactions could be achieved. More importantly, in delicate supramolecular frameworks, not only can unimolecular nonradiative transitions be suppressed, but the annoying intermolecular quenching can also be relieved with distanced electron-rich segments (shown in Fig. 2e).[50]

Intermolecular exciton quenching in OLEDs is dominated by electron-exchange interactions of triplet excitons and is

Open Access Article. Published on 22 febbraio 2022. Downloaded on 08/05/2026 07:17:27.
This article is licensed under a Creative Commons Attribution-NonCommercial 3.0 Unported Licence.

generally serious between TADF emitters based on intramolecular charge-transfer (CT) transitions, while there is another type of TADF emitter based on intermolecular CT transitions, which is an exciplex. Intermolecular mutual collisions in the exciplex favor the recombination of excitons rather than exciton annihilation. In a neat film containing a single material with molecular configurations such as D–spacer–A structures (shown in Fig. 2f), a space-enough and conjugation-forbidden diphenyl ether linkage can effectively suppress the intramolecular charge-transfer (CT) transition while forming an exciplex-type emitter *via* the intermolecular CT transition.[51]

3. TADF emitters for nondoped OLEDs

3.1. Cyano-substituted aromatics as acceptors

Cyano (CN)-substituted aromatics have been widely used to construct TADF emitters due to their strong electron-withdrawing abilities and high chemical stabilities. The molecular structures of CN-based TADF emitters are shown in Fig. 3, and the corresponding key parameters of their nondoped devices are summarized in Table 1. Grazulevicius *et al.*[52] designed five benzonitrile (BN)-based TADF emitters **1–5** with symmetrical donor–acceptor–donor (D–A–D) and asymmetrical donor–acceptor–donor* (D–A–D*) molecular structures to carefully study the influence of different substitution patterns on device performance. Charge transport tests show that molecular structures significantly affect the charge carrier mobilities, which can be ascribed to the different molecular packings in amorphous states. However, their nondoped devices all show poor results with maximum external quantum efficiencies (EQEs) below 5.0% because their electron-withdrawing core BN moiety is unprotected.

Yang *et al.*[53] reported a series of sky-blue TADF emitters **6–8** by linking di-*tert*-butylcarbazole (*t*BuCz) and difluorocyanobenzene (CNDF) groups on the phenyl bridge simultaneously with mutual *ortho*-positions. The large steric *t*BuCz groups not only effectively protect the electron-withdrawing core CNDF moieties but also favor the coexistence of through-space CT and through-bond CT. Compared with the large ΔE_{ST} values of 0.24 eV and 0.21 eV for **6** and **7**, the highly twisted multi-(D/A) molecular structure of **8** can not only effectively lower its ΔE_{ST} (0.03 eV) but also suppress the intermolecular close π–π packing. As a result, the **8** amorphous neat film gives a high PLQY of 0.76. Therefore, the **8**-based solution-processed nondoped device realizes sky-blue emission with a peak at 484 nm and a maximum EQE of 21.0%.

Wang *et al.*[54] also proposed a facile and efficient molecular design strategy for shielding the BN moiety with carbazole derivatives (Cz and *t*BuCz). In their newly designed compounds **9** and **10**, 9,9-diphenylacridan (DPAc) and BN were the D and A groups, respectively. Introduction of Cz and *t*BuCz groups as the protective units can not only effectively isolate the triplet excited states but also enhance the rigidity of the molecular skeletons and decrease molecular vibrations/rotations. Thus, in nondoped OLEDs, **9** and **10** achieved high performance with

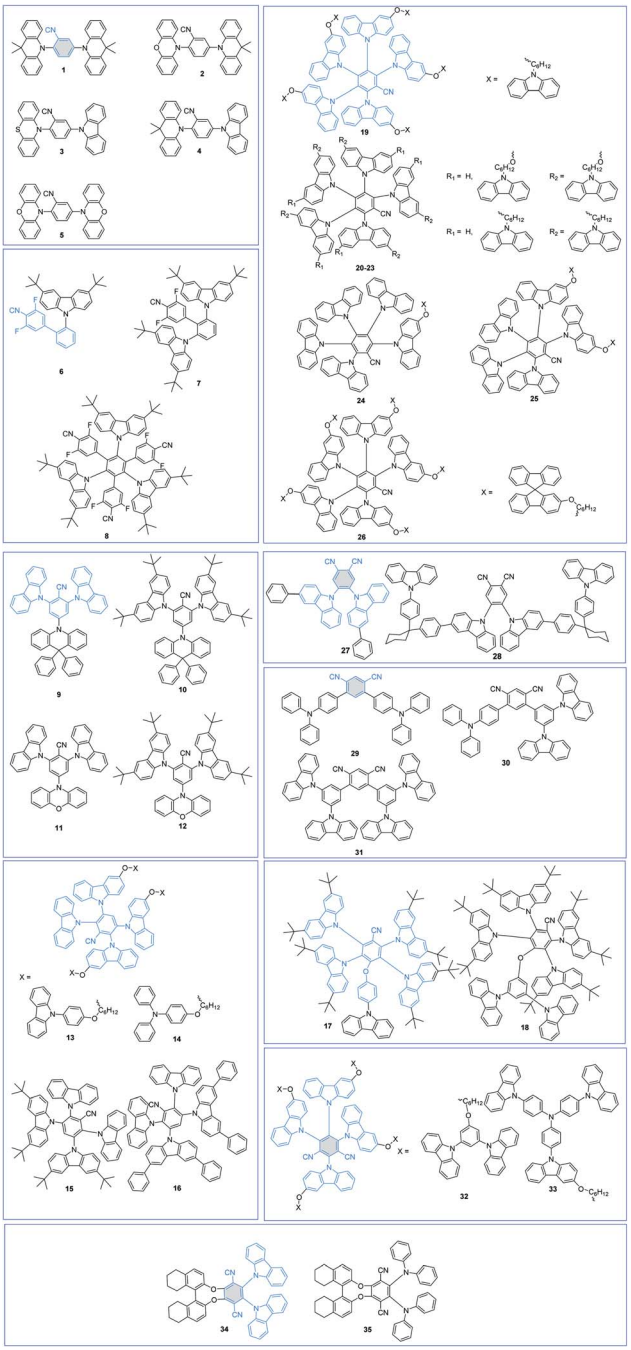

Fig. 3 Molecular structures of cyano-based TADF emitters for nondoped OLEDs.

maximum EQEs of 10.1% and 20.0% and CIE coordinates of (0.16, 0.19) and (0.16, 0.26), respectively. In particular, the inferior performance of the **9**-based device can be reasonably attributed to its poorer carrier mobilities. Based on the results, we can notice that a more delicate balance between the protection functions and carrier mobilities is needed. By further replacing the DPAc unit with a more electron-rich phenoxazine (PXZ) unit, two novel TADF emitters **11** and **12** were also synthesized.[55] Nevertheless, due to the unprotected rigid and planar PXZ unit, which is prone to close intermolecular

© 2022 The Author(s). Published by the Royal Society of Chemistry

Open Access Article. Published on 22 febbraio 2022. Downloaded on 08/05/2026 07:17:27.
This article is licensed under a Creative Commons Attribution-NonCommercial 3.0 Unported Licence.

Table 1 Photoluminescence (PL) and electroluminescence (EL) properties of cyano-based TADF emitters in nondoped films

	PL			EL						
						CE/PE/EQE [cd A^{-1}/lm W^{-1}/%]				
	PLQY	τ_p [ns]	τ_d [μs]	Peak [nm]	V_{on}[a] [V]	Maximum	@10^3 cd m^{-2}	Roll-off[b] [%]	CIE (x,y)	Ref.
1	0.42	—	—	~477	3.6	5.3/3.6/2.5	—	—	(0.19, 0.29)	52
2	0.26	—	—	~525	3.4	16.3/12.2/5.0	—	—	(0.31, 0.57)	
3	0.11	—	—	~540	4.4	5.2/3.5/1.6	—	—	(0.35, 0.52)	
4	0.39	—	—	~477	4.5	8.4/4.9/4.1	—	—	(0.18, 0.27)	
5	0.18	—	—	~534	3.6	7.7/6.0/2.4	—	—	(0.34, 0.55)	
6	0.42	17.0	—	466	10.1	3.6/1.4/2.6	—	—	(0.16, 0.18)	53
7	0.19	14.1	—	466	5.7	5.0/2.2/3.7	—	—	(0.16, 0.17)	
8	0.76	21.3	—	484	6.3	46.4/20.8/21.0	—	—	(0.19, 0.35)	
9	0.57	21.4	5.5	476	3.2	41.4/35.4/20.0	—	—	(0.16, 0.26)	54
10	0.55	15.8	7.1	460	5.4	10.1/7.1/10.1	—	—	(0.16, 0.19)	
11	0.48	18.0	0.8	568	2.4	38.1/42.6/13.6	—/—/12.8	5.9	(0.46, 0.52)	55
12	0.50	21.6	1.1	—	3.7	21.1/14.7/6.6	—/—/3.9	41.0	(0.36, 0.56)	
13	0.63	15.0	3.3	—	2.8	45.2/35.5/22.6	—/—/18.9	16.4	(0.16, 0.29)	58
14	0.40	15.0	2.5	—	—	—	—	—	—	
15	0.66	15.7	9.8	470	2.7	31.1/—/21.6	18.9/—/10.8	50.0	(0.17, 0.25)	59
16	0.45	17.4	5.1	480	6.7	8.5/—/3.9	7.1/—/3.3	15.4	(0.20, 0.33)	
17	0.39	—	—	496	3.7	18.4/11.6/5.9	12.1/—/—	—	(0.22, 0.39)	60
18	0.61	—	—	484	3.5	24.9/19.5/8.0	14.3/—/—	—	(0.18, 0.31)	
19	0.52	—	—	510	3.1	49.7/45.9/17.1	46.8/—/—	—	(0.26, 0.52)	63
20	0.56	6.9	2.4	523	2.8	40.2/31.5/13.8	32.6/—/—	—	(0.37, 0.58)	64
21	0.77	6.3	4.2	541	3.2	56.2/45.2/17.4	48.6/—/—	—	(0.40, 0.57)	
22	0.59	8.7	3.6	516	3.0	41.7/34.5/14.4	39.9/—/—	—	(0.25, 0.55)	
23	0.80	5.5	4.5	515	3.6	63.0/48.7/20.4	43.5/—/—	—	(0.25, 0.52)	
24	0.38	38	3.1	—	3.4	21.9/17.2/7.3	—	—	(0.28, 0.54)	65
25	0.46	56	3.8	—	3.2	40.7/31.9/13.9	—	—	(0.27, 0.54)	
26	0.70	77	4.5	508	3.1	58.7/46.2/20.1	—	—	(0.27, 0.53)	
27	0.60	24.2	6.1	524	3.6	22.3/17.5/7.5	—	—	(0.31, 0.52)	66
28	0.89	25.2	6.9	524	4.2	40.8/28.5/13.4	—	—	(0.33, 0.54)	
29	0.84	8.6	—	520	2.6	11.8/10.3/3.5	—/—/2.7	22.8	(0.20, 0.33)	67
30	1.00	9.1	—	520	2.8	15.7/12.0/4.9	—/—/3.7	24.5	(0.29, 0.61)	
31	0.46	13.9	—	520	3.0	26.6/22.4/8.3	—/—/6.5	21.7	(0.30, 0.58)	
32	0.08	22.0	1.4	552	4.4	1.4/0.9/0.5	—	—	(0.46, 0.52)	69
33	0.90	16.0	1.0	548	2.7	44.5/46.6/16.5	30.5/19.1/11.3	31.5	(0.42, 0.55)	
34	0.81	8.9	6.1	562	3.5	47.8/34.6/14.0	46.6/—/13.6	2.8	—	70
35	0.78	9.8	8.3	560	3.6	23.0/16.8/6.6	18.4/—/5.4	18.2	—	71

[a] Turn-on voltage at a luminance of 1 cd m^{-2}. [b] $EQE_{roll\text{-}off} = (EQE_{max} - EQE_{1000})/EQE_{max}$.

packing, the **11**- and **12**-based nondoped OLEDs show poor performance with maximum EQEs of 6.6% and 13.6%, respectively, which are much lower than those of DPAc-based emitters. These results further demonstrate that both D and A moieties should be well protected to shield potential intermolecular charge exchange.

Since the pioneering work of Adachi *et al.*[3] in 2012, carbazolyl dicyanobenzene (CDCB) derivatives have been carefully studied. As a member of the CDCB family, 2,3,5,6-tetra(9*H*-carbazol-9-yl) benzonitrile (4CzBN) and its derivatives have been widely used to construct high-performance blue TADF emitters.[56,57] By using the self-host molecular design strategy, Sun *et al.*[58] reported two 4CzBN-based TADF emitters **13** and **14** for fully solution-processed blue nondoped devices. Both emitters possess identical emissive cores but different bulky shielding groups. As displayed in Fig. 4, unlike the formation of the **14**-based electromer state during electroexcitation, the rigid phenylcarbazole (PCz) unit in **13** can efficiently block such energy leakage. As a result, the **13**-based fully solution-processed blue OLED realizes a maximum EQE of 22.6%, which is almost 20 times higher than that of the **14**-based OLED. With the same emission core, Tang *et al.*[59] also reported two 4CzBN-based blue TADF emitters **15** and **16** by introducing steric groups. Both emitters exhibit blue emission at 464 nm with a $CIE_y < 0.2$ and an EQE over 20% in doped devices. Meanwhile, compared with the steric *tert*-butyl (*t*Bu) group in **15**, the terminal phenyl group in **16** can effectively weaken the intermolecular π–π packing in the solid-state film and significantly enhance the PLQY. Therefore, the **16**-based nondoped device achieves a maximum EQE of 21.6% with an extremely low turn-on voltage (V_{on}) of 2.7 V. Sun *et al.*[60] also synthesized two 4CzBN-based blue TADF emitters **17** and **18** with the host-σ-guest molecular configuration for solution-processed nondoped OLEDs. The oxygen bridge-linked host

Open Access Article. Published on 22 febbraio 2022. Downloaded on 08/05/2026 07:17:27.
This article is licensed under a Creative Commons Attribution-NonCommercial 3.0 Unported Licence.

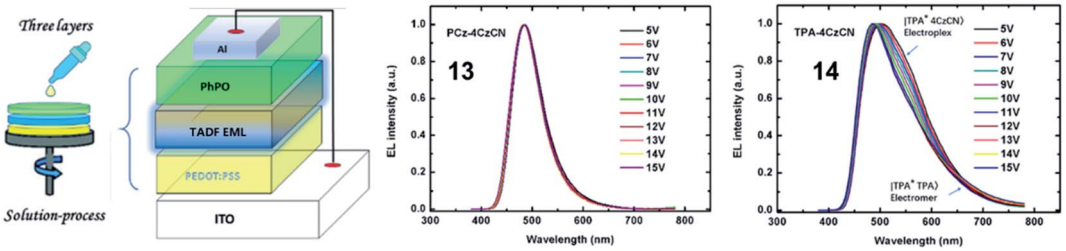

Fig. 4 Device structure of the fully solution-processed devices and normalized EL spectra at different voltages. Reproduced from ref. 58 with permission. Copyright 2019 American Chemical Society.

can not only suppress triplet exciton quenching between guest units but also improve the carrier transport ability.

As another representative member of the CDCB family, 2,3,4,5,6-penta(9*H*-carbazol-9-yl)benzonitrile (5CzBN) is an excellent precursor to exploit TADF emitters for efficient sky-blue nondoped devices.[61,62] By applying a self-host molecular design strategy, Sun *et al.*[63] conveniently constructed TADF emitter **19** for solution-processed nondoped OLEDs. The alkyl chain-linked Cz units can sufficiently encapsulate the 5CzBN emission core and effectively suppress intermolecular interaction-induced exciton quenching. Therefore, compared with the low PLQY of 0.21 for precursor 5CzBN, the **19** amorphous neat film exhibits a higher PLQY of 0.52. By further applying **19** as the pure EML, the corresponding solution-processed nondoped device achieves a low V_{on} of 3.1 V and a high maximum EQE of 17.1%. To enhance device performance, they further decorated precursor 5CzBN with different peripheral functional groups (**20–23**).[64] Sufficient Cz decoration can effectively encapsulate the central chromophore and thus prevent these units from being redissolved by isopropanol. Therefore, they can be used in fully solution-processed devices with a device structure of ITO/PEDOT:PSS (40 nm)/EML (40 nm)/PO-T2T (30 nm)/Cs_2CO_3 (2 nm)/Al (100 nm). Compared with their monosubstituted counterparts (**20** and **22**), the disubstituted compounds (**21** and **23**) show superior device performances, which can be ascribed to the well-protected TADF emission core. Tang *et al.*[65] also tried to decorate the 5CzBN core with different numbers of alkyl chain-linked spirobifluorene (SPF) groups (**24–26**). All these emitters show obvious AIDF characteristics. Moreover, with increasing flexible dendron numbers, intermolecular interactions can be well restricted. Thus, the **26** pristine film shows better resistance to isopropyl alcohol than the others, benefiting the solution fabrication process. The corresponding fully solution-processed nondoped device achieves a maximum EQE of 20.1%. All these results suggest that sufficiently peripheral decorations act as a feasible method to construct TADF emitters for fully solution-processed devices.

To further broaden the luminescence range of CN-based TADF materials, adjusting the numbers and positions of the CN groups is a feasible method. 4,5-di(9*H*-carbazol-9-yl) phthalonitrile (2CzPN) is a well-known blue TADF emitter; however, due to its poor solubility, it is rarely used in solution-processed devices. To exploit 2CzPN-based materials for solution-processed OLEDs, Choi *et al.*[66] reported a novel AIE and TADF-active triad **28** and a control compound, 4,5-bis(3-phenyl-9*H*-carbazol-9-yl)phthalonitrile (**27**). Compared with the parent molecule (**27**), introducing PCz and nonconjugated cyclohexane units as the host and bridge moieties in **28**, respectively, can effectively enlarge the intermolecular distance without affecting the electroluminescence (EL) spectrum. In solution-processed nondoped OLEDs, they exhibit nearly identical green EL emissions with peaks at 524 nm, while the maximum EQE of **28** (13.4%) is significantly better than that of **27** (7.5%).

Wang *et al.*[67] also applied the isophthalonitrile moiety, in which two cyano groups are at the *meta*-positions, to design D–π–A-type TADF materials **29–31**. The nondoped device using Cz-decorated **31** as the EML shows a superior device performance to the others, which can be reasonably ascribed to the following reasons: (1) relatively high hole mobility of the TPA group; (2) the rigid and twisted molecular conformation, which can effectively suppress the aggregation-caused quenching (ACQ) effect. Likewise, 2,4,5,6-tetra(9*H*-carbazol-9-yl)isophthalonitrile (4CzIPN) is also decorated for nondoped devices due to its excellent device performance. Nevertheless, it shows a high concentration sensitivity and poor nondoped device efficiency due to the tendency of forming Cz-based dimers.[68] To achieve 4CzIPN-based high-performance nondoped devices, Jiang *et al.*[69] connected the emission core 4CzIPN with the host matrix *via* flexible alkyl chains by applying a self-host molecular design strategy. In particular, the peripherally decorated 1,3-di(9*H*-carbazol-9-yl) benzene/tris(4-(9*H*-carbazol-9-yl)phenyl)amine (*m*CP/TCTA) moiety can form a high triplet level interfacial exciplex with the electron-transporting layer (ETL). Due to the extra intramolecular exciplex under electrical stress, the **33**-based nondoped device exhibits a much lower device performance than **32**.

Circularly polarized luminescence (CPL) has great applications in optical data storage, quantum computing, bio-responsive imaging, liquid crystal displays, and backlights in 3D displays. Pan *et al.*[70,71] developed a series of chiral TADF emitters **34** and **35** by merging chiral (*R*/*S*)-octahydrobinaphthyl ((*R*/*S*)-OBN) moieties with effective CN-based TADF skeletons. Similar to the abovementioned TPA/Cz-based compounds,[67] the rigid and twisted molecular conformation of **34** effectively suppresses triplet exciton quenching.

3.2. Carbonyl-substituted aromatics as acceptors

Aromatic units containing strong electron-withdrawing carbonyl groups in the center, such as benzophenone (BP)

© 2022 The Author(s). Published by the Royal Society of Chemistry

Open Access Article. Published on 22 febbraio 2022. Downloaded on 08/05/2026 07:17:27.
This article is licensed under a Creative Commons Attribution-NonCommercial 3.0 Unported Licence.

and its derivatives, have been widely used as the A unit for designing TADF emitters. The molecular structures of BP-based TADF emitters are shown in Fig. 5, and the corresponding key parameters of the nondoped devices are summarized in Table 2. Adachi *et al.*[72] reported the first D–A–D type BP-based TADF emitter **36** for high-performance nondoped OLEDs. A rigid and steric 9,9-dimethyl-9,10-dihydroacridine (DMAC) moiety can effectively restrain long-lived triplet exciton quenching, and its amorphous neat film thus displays a high PLQY of 0.85 and a short delayed lifetime (τ_d) of 2.7 μs, guaranteeing efficient nondoped devices. As summarized in Table 2, the **36**-based nondoped OLED exhibits a superior performance with a maximum EQE of 18.9% with mild efficiency roll-off at high luminance. Yang *et al.*[73] further modified precursor **36** by encapsulating the DMAC moiety with *t*BuCz and 3,6-bis-(3,6-di-*tert*-butylcarbazol-9-yl)-carbazole (*t*BuCz2) groups and developed two novel TADF dendrimers **37** and **38** for solution-processed nondoped devices. Both dendrimers exhibit good thermal and morphological stabilities, guaranteeing homogeneous and stable amorphous thin films *via* solution-processed fabrication. Owing to the significantly decreased carrier transport arising from the large steric hindrance of the *t*BuCz2 unit, the **37**-based device exhibits a much lower driving voltage of 4.8 V at a luminance of 10 cd m^{-2} than that of **38** (7.7 V). Moreover, the nondoped device using **37** as the EML shows a maximum EQE of 12.0%, three times larger than that of the **38**-based device. Cheng *et al.*[74] also reported a series of TADF polymers **39** by using conjugated Cz/acridine moieties as the backbone and BP as the pendant A moiety. The solution-processed nondoped device achieves a high device performance with a very mild efficiency roll-off.

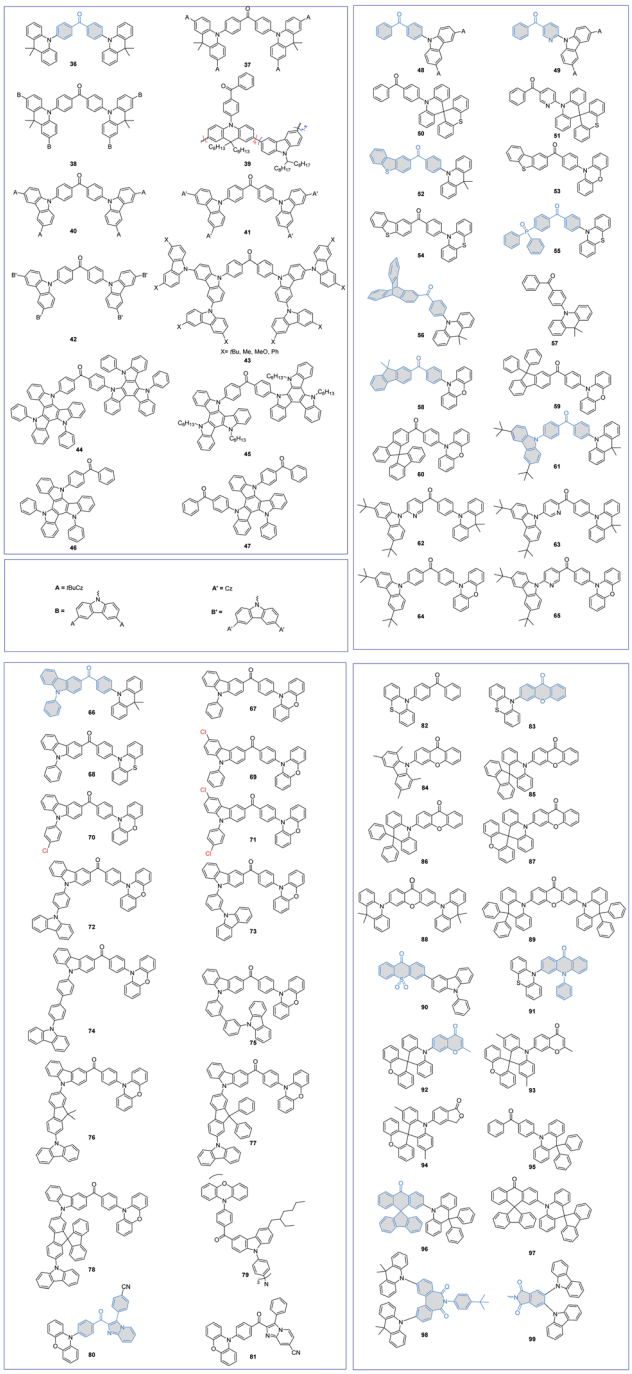

Fig. 5 Molecular structures of carbonyl-based TADF emitters for nondoped OLEDs.

By replacing the DMAC moiety with a soluble *t*BuCz2 moiety, Sun *et al.*[75] synthesized a novel dendronized TADF emitter (**40**) for solution-processed nondoped green OLEDs. Although the **40**-based neat film exhibits a high PLQY (0.65) and a small ΔE_{ST} (0.08 eV), its solution-processed device shows a poor performance with a maximum EQE of 4.3%, which may be ascribed to the decreased bipolar carrier transport.[54] Fujita *et al.*[76] also designed a series of BP-based AIDF dendrimers (**41** and **42**) for solution-processed nondoped devices. By further modulating the terminal groups (**43**),[77] they found that the terminal groups can dramatically alter the photophysical properties of dendritic TADF emitters. The introduction of *t*Bu and phenyl groups favors the AIE character, while the introduction of a methoxy group results in emission quenching. Thus, it is important to choose suitable terminal functional groups for designing TADF emitters for solution-processed nondoped devices.

Triazatruxene (TAT), a planar conjugated system with three fused carbazole fragments that share a benzene ring, acted as a powerful D group to construct TADF emitters. Wang *et al.*[78] first characterized two TAT-based TADF emitters **44** and **45** for solution-processed devices. Compared with the long alkyl-decorated TAT unit in **45**, the four peripheral phenyl substituents in **44** can effectively enlarge the distance of adjacent triplet excitons. Therefore, although both emitters realize identical device performances with maximum EQEs of approximately 6.0%, the **45**-based device displays a more serious efficiency roll-off at high luminance. To further improve the device performance, they also synthesized two asymmetrical D–A-type AIDF emitters **46** and **47** by using phenyl-substituted TAT and BP as the D and A groups, respectively.[79] The **47**-based solution-processed nondoped device exhibits a higher device efficiency than **46**, possibly due to the balanced carrier transport caused by the introduction of one more BP unit.

Compared with D–A–D-type symmetric molecular structures, BP-based TADF materials with unsymmetrical structures have

Open Access Article. Published on 22 febbraio 2022. Downloaded on 08/05/2026 07:17:27.
This article is licensed under a Creative Commons Attribution-NonCommercial 3.0 Unported Licence.

Table 2 PL and EL properties of carbonyl-based TADF emitters in nondoped films

	PL			EL						
						CE/PE/EQE [cd A^{-1}/lm W^{-1}/%]				
	PLQY	τ_p [ns]	τ_d [μs]	Peak [nm]	V_{on}[a] [V]	Maximum	@10^3 cd m^{-2}	Roll-off[b] [%]	CIE (x,y)	Ref.
36	0.85	—	2.7	510	2.6	—/—/18.9	—/—/18.0	4.8	(0.26, 0.55)	72
37	0.77	—	—	546	—	—/—/12.0	—/—/11.9	0.8	(0.38, 0.56)	73
38	0.75	—	—	522	—	—/—/5.2	—/—/4.1	21.1	(0.32, 0.51)	
39	0.77	22.0	1.3	∼550	2.6	60.5/61.2/18.1	59.4/50.4/17.8	1.6	(0.40, 0.56)	74
40	0.65	0.45	0.6	506	4.5	9.2/—/4.3	—	—	(0.26, 0.46)	75
41	0.33	10.4	2.7	500	3.4	14.0/11.5/5.7	—	—	(0.26, 0.48)	76
42	0.21	20.8	3.4	516	3.7	7.7/5.7/2.9	—	—	(0.31, 0.50)	
43	0.74	11.9	2.2	∼504	2.7	46.6/40.7/17.0	—/—/13.8	18.8	(0.27, 0.52)	77
44	0.24	40.8	0.9	∼541	2.7	18.9/19.2/6.0	18.0/16.1/5.8	3.3	(0.38, 0.55)	78
45	0.22	53.5	0.9	∼551	2.6	17.8/20.0/5.9	12.0/10.2/4.8	18.6	(0.41, 0.54)	
46	0.51	46.7	0.8	∼530	2.5	20.9/21.8/6.4	18.5/17.1/5.4	15.6	—	79
47	0.44	37.3	0.5	∼530	2.5	32.3/33.0/9.8	31.2/31.9/9.7	1.0	—	
48	0.22	20.0	1.3	492	4.4	9.7/6.1/4.2	—/—/1.3	69.0	(0.19, 0.36)	80
49	0.37	20.4	1.0	508	4.4	24.0/15.6/8.5	—/—/4.5	47.0	(0.26, 0.50)	
50	0.57	25.9	5.0	494	3.2	34.7/30.1/14.2	—/—/10.8	23.9	(0.20, 0.39)	
51	0.72	29.8	1.9	512	3.2	56.4/43.5/18.7	—/—/17.9	4.3	(0.28, 0.53)	
52	0.80	40.4	2.9	516	2.7	43.3/35.7/14.2	43.1/33.1/14.2	0.0	(0.26, 0.55)	81
53	0.38	38.3	1.8	557	2.9	26.6/27.9/9.2	19.6/11.3/6.8	26.1	(0.43, 0.54)	82
54	0.40	27.6	1.3	563	2.7	26.5/29.1/9.7	23.5/15.4/8.5	12.4	(0.45, 0.53)	
55	—	—	—	586	5.4	37.6/14.8/16.7	26.9/10.8/11.8	29.3	—	83
56	0.69	—	—	501	2.8	42.7/39.8/15.6	41.0/27.0/15.0	3.8	(0.25, 0.48)	84
57	0.37	—	—	503	3.9	18.2/14.1/6.6	13.1/5.5/4.8	27.3	(0.26, 0.47)	
58	0.45	30.2	1.4	∼560	2.7	39.9/39.0/13.3	37.4/24.0/12.5	6.0	(0.44, 0.54)	85
59	0.49	27.9	1.1	∼564	2.6	41.6/45.0/14.3	41.4/26.0/14.1	1.4	(0.46, 0.53)	
60	0.46	27.5	1.1	∼562	2.5	36.8/37.9/12.3	36.7/28.8/12.2	0.8	(0.46, 0.53)	
61	0.47	19.1	1.0	499	4.5	14.3/6.4/6.7	—	—	(0.28, 0.47)	86
62	0.67	7.2	1.4	532	4.2	35.4/15.9/11.4	—	—	(0.34, 0.51)	
63	0.53	12.7	1.1	544	4.3	23.8/10.7/9.1	—	—	(0.39, 0.56)	
64	0.33	13.5	0.9	545	4.8	12.4/4.3/4.8	—	—	(0.41, 0.55)	
65	0.48	8.4	1.1	572	4.6	21.6/6.8/9.4	—	—	(0.47, 0.51)	
66	0.45	19.1	5.7	502	2.7	41.6/37.9/15.0	41.5/32.6/14.9	0.7	(0.23, 0.49)	44
67	0.67	21.9	5.5	548	2.5	59.1/65.7/18.4	58.4/49.7/18.2	1.1	(0.40, 0.57)	
68	0.58	23.5	2.1	554	2.5	46.1/55.7/15.3	38.4/30.2/12.7	17.0	(0.42, 0.55)	
69	0.73	22.2	0.8	540	2.8	76.6/75.2/21.7	69.8/52.2/19.8	8.8	(0.38, 0.58)	22
70	0.70	22.2	0.7	537	2.6	72.5/53.5/20.4	68.5/43.1/19.4	4.9	(0.37, 0.59)	
71	0.73	22.1	0.4	541	2.8	72.1/65.4/20.6	69.0/51.6/19.7	4.4	(0.39, 0.58)	
72	0.69	22.4	2.6	548	2.5	72.9/81.8/22.6	—/—/22.0	2.6	(0.39, 0.57)	87
73	0.72	21.1	2.4	546	2.5	69.0/75.0/21.4	—/—/20.9	2.3	(0.39, 0.57)	
74	0.66	23.7	2.3	542	2.5	72.3/79.0/22.1	—/—/22.1	0.0	(0.39, 0.57)	
75	0.71	23.0	2.4	542	2.5	70.4/76.5/21.8	—/—/21.8	0.0	(0.38, 0.57)	
76	0.88	22.3	2.1	540	2.6	62.2/63.7/19.0	60.7/47.5/18.5	2.6	(0.39, 0.57)	88
77	0.89	22.2	1.7	544	2.5	61.1/67.4/18.5	60.3/60.1/18.2	1.6	(0.38, 0.57)	
78	0.40	18.9	0.9	548	2.7	10.8/8.6/3.3	10.7/8.1/3.2	3.0	(0.40, 0.56)	
79	0.66	12.5	0.8	535	4.2	37.2/14.6/12.1	—	—	(0.38, 0.56)	89
80	0.31	17.5	0.4	592	4.8	10.7/4.8/4.9	7.2/2.2/3.2	34.7	(0.54, 0.45)	90
81	0.32	15.0	0.2	606	3.0	6.5/4.0/3.7	6.3/3.3/3.5	5.4	(0.57, 0.42)	
82	0.31	23.0	1.4	577	3.0	—/—/7.6	—/—/∼6.1	19.7	—	91
83	0.53	29.0	1.9	553	3.0	—/—/11.1	—/—/∼4.2	62.2	—	
84	0.50	33.3	1.2	488	3.9	—/—/5.2	—/—/2.2	57.7	—	46
85	0.82	23.0	2.0	497	3.6	—/—/12.6	—/—/9.5	24.6	—	
86	0.92	35.0	2.2	488	3.5	—/—/11.2	—/—/5.9	47.3	—	
87	0.84	22.7	5.3	488	3.8	—/—/14.1	—/—/10.5	25.5	—	
88	0.96	43.3	1.4	526	2.9	74.0/67.0/21.0	74.0/61.0/21.0	0.0	(0.31, 0.61)	92
89	0.94	34.6	1.9	496	3.5	55.0/42.0/21.0	46.0/27.0/18.0	14.3	(0.22, 0.49)	
90	—	—	112	520	—	69.0/50.0/22.6	—/—/∼4.0	82.3	—	93
91	0.76	10.0	1.7	549	2.4	50.5/60.0/17.1	42.7/26.5/13.8	19.3	(0.42, 0.55)	94
92	0.53	25.0	2.8	462	3.6	—/14.7/12.1	—/—/7.1	41.3	(0.15, 0.19)	95
93	0.71	33.0	2.8	478	3.3	—/25.7/15.0	—/—/11.1	26.0	(0.16, 0.29)	

© 2022 The Author(s). Published by the Royal Society of Chemistry

Open Access Article. Published on 22 febbraio 2022. Downloaded on 08/05/2026 07:17:27.
This article is licensed under a Creative Commons Attribution-NonCommercial 3.0 Unported Licence.

Table 2 (*Contd.*)

	PL			EL						
						CE/PE/EQE [cd A^{-1}/lm W^{-1}/%]				
	PLQY	τ_p [ns]	τ_d [μs]	Peak [nm]	V_{on}[a] [V]	Maximum	@10^3 cd m^{-2}	Roll-off[b] [%]	CIE (x,y)	Ref.
94	0.78	24.0	3.8	478	3.0	—/31.5/16.2	—/—/12	25.9	(0.17, 0.29)	
95	0.47	17.9	5.3	496	3.0	32.7/34.3/12.9	13.8/10.1/4.3	66.7	(0.21, 0.42)	96
96	0.93	24.4	2.5	504	3.1	63.7/54.1/22.8	61.4/49.9/22.4	1.8	(0.23, 0.50)	
97	0.98	24.9	1.3	516	3.1	65.7/51.6/21.3	64/53.4/20.8	2.3	(0.27, 0.56)	
98	0.96	37.2	3.1	508	2.9	—/59.7/24.9	—/46.0/21.7	12.8	(0.24, 0.49)	97
99	0.55	—	—	517	3.6	17.6/13.9/5.9	—	—	(0.30, 0.51)	98

[a] Turn-on voltage at a luminance of 1 cd m^{-2}. [b] $EQE_{roll\text{-}off} = (EQE_{max} - EQE_{1000})/EQE_{max}$.

drawn more attention due to the advantages of effective regulation of molecular packing and bipolar carrier transport. Su *et al.*[80] developed a series of BP-based D–A-type TADF materials **48–51**. Compared with the parent BP moiety, the pyridine-containing 3-benzoylpyridine group can significantly enhance the molecular rigidity by forming an intramolecular hydrogen bond. Therefore, pyridine-decorated **49** and **51** exhibit slightly reduced ΔE_{ST}s and obviously improved PLQYs compared with their BP-based counterparts (**48** and **50**). Moreover, the rigid 10*H*-spiro(acridine-9,9′-thioxanthene) (TXDMAc) group can effectively shield the electron-rich acridine core and restrict concentration quenching. As a result, the nondoped OLEDs obtained by using TXDMAc-based TADF emitters **50** and **51** as the EMLs show superior performances, with maximum EQEs of 14.2% and 18.7%, much higher than those of Cz-based OLEDs (maximum EQEs of 4.2% and 8.5%, respectively, for **48** and **49**).

Tang *et al.*[81] also developed a D–A–D′-type AIDF emitter **52** by using DMAC and dibenzothiophene (DBT) moieties as the D and D′, respectively. The DMAC-BP segment is anticipated to form a twisted molecular conformation to realize AIE and TADF properties, while planar DBT may help to increase the charge-transporting ability. Therefore, the **52** neat film displays a high PLQY of 0.80 and a smaller ΔE_{ST} of 0.08 eV, benefiting the utilization of electrogenerated excitons. By further replacing the DMAC moiety with electron-rich PXZ and phenothiazine (PTZ) moieties, two analog AIDF emitters **53** and **54** were also synthesized.[82] However, since unprotected PXZ/PTZ groups tend to aggregate in solid-states and can induce severe triplet exciton quenching, their nondoped device performance is much worse than that of **52** (maximum EQEs of 14.2%, 9.2%, and 9.7% for **52**, **53**, and **54**, respectively).

By introducing a diphenylphosphoryl (DPO) unit as the A′, Chi *et al.* designed an unsymmetrical D–A–A′-type TADF emitter **55**.[83] The corresponding nondoped device demonstrates orange emission with a peak at 586 nm and a maximum EQE of 16.7%, which is among the best performances of TADF-based nondoped OLEDs in the orange-red region.

To enhance the rigidity of the BP skeleton, Lu *et al.*[84] prepared a novel triptycene-fused BP moiety, and a D–A-type TADF emitter **56** was then designed. For comparison, D–A-type emitter **57** was also synthesized by using DMAC and BP as the D and A moieties, respectively. Introducing a rigid and steric triptycene scaffold can not only strengthen the molecular rigidity but also effectively restrict intermolecular interactions in aggregated states. Therefore, the nondoped device using **56** as the EML achieves a maximum EQE of 15.6%, much higher than that of **57** (a maximum EQE of 4.8%).

Tang *et al.*[85] also used steric fluorene derivatives to decorate the precursor BP-PXZ and developed three AIDF emitters **58–60** for nondoped OLEDs. The highly twisted conformation with large sterically hindered fluorene groups can effectively suppress the short-range Dexter energy transfer (DET) process at high exciton concentrations, thus significantly relieving the annihilation of triplet excitons. On this account, the corresponding nondoped OLEDs all exhibit good device performance with maximum EQEs over 12.3%.

Qi *et al.*[86] demonstrated a class of efficient AIDF materials **61–65** bearing pyridine-decorated BP as the A moiety and *t*BuCz/DMAC/PXZ as the D moieties. The presence of intramolecular hydrogen bonding can effectively suppress nonradiative decay and improve the luminescence efficiency of the aggregated solid-state. Meanwhile, compared with the planar PXZ unit (**64** and **65**), the steric DMAC group in **61–63** can effectively restrict the intermolecular π–π packing.

By replacing *t*BuCz with a 9-phenyl-9*H*-carbazole (PCz) moiety, three unsymmetrical AIDF emitters **66–68** were synthesized by Tang *et al.*[44] As shown in Fig. 6, the PCz moiety can effectively impede close molecular packing and weaken intermolecular interactions. Therefore, concentration-induced emission quenching and exciton annihilation can be greatly suppressed. Meanwhile, the electron-rich PXZ group in **67** favors a smaller ΔE_{ST} (0.024 eV) and shorter lifetime τ_d (2.1 μs) than those of **66** (0.07 eV and 2.7 μs) in neat film states. Therefore, the **67**-based nondoped device shows a superior performance with a maximum EQE of 18.4% compared to **66** (maximum EQE of 15.0%). To further explore the methods to alleviate the concentration quenching of PXZ-based TADF emitters, they proposed accelerating the RISC process by introducing heavy atoms (**69–71**).[22] Compared with the precursor AIDF emitter **67**, chlorine-modified **69–71** exhibit

Open Access Article. Published on 22 febbraio 2022. Downloaded on 08/05/2026 07:17:27.
This article is licensed under a Creative Commons Attribution-NonCommercial 3.0 Unported Licence.

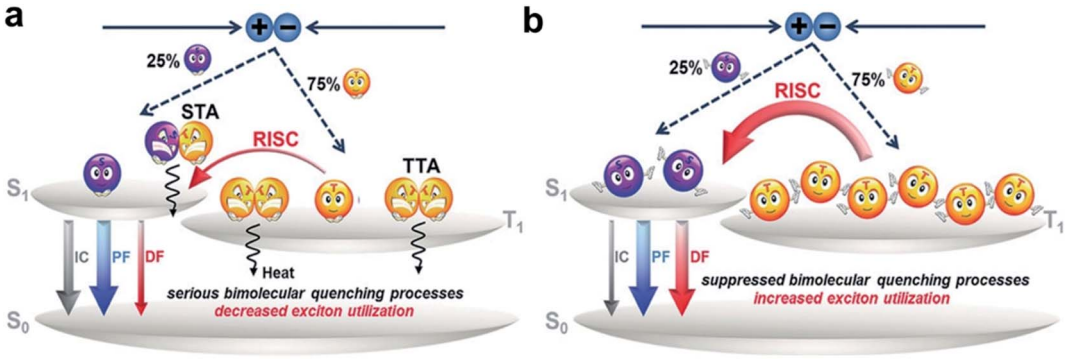

Fig. 6 Schematic illustration of the main exciton dynamic processes for (a) a conventional luminogen with delayed fluorescence and (b) an AIDF emitter in nondoped OLEDs. Reproduced from ref. 44 with permission. Copyright 2017 Wiley-VCH.

higher PLQYs and shorter τ_d values, which can be attributed to the heavy atom effect that greatly increases the SOC values and significantly accelerates the RISC process. As a result, their nondoped OLEDs exhibit outstanding device performances with excellent maximum EQEs over 20.4%. To further improve the device performance, they also proposed a self-host molecular design strategy by grafting the AIDF 4-(phenoxazin-10-yl) benzoyl moiety to common host materials, including 1,4-di(carbazol-9-yl)benzene (DCB), CBP, *m*CP, and 3,3′-di(carbazol-9-yl)biphenyl (*m*CBP), and developed materials **72–75**.[87] The photophysical and electrochemical behaviors of **72–75** are very similar and seem to be mainly determined by the parent 4-(phenoxazin-10-yl)benzoyl fragment. The nondoped OLEDs using these generated luminogens exhibit outstanding performances with excellent maximum EQEs (22.1–22.6%) and high efficiency stability. All these results demonstrate that introducing a host matrix can effectively relieve triplet exciton annihilation without affecting the EL emission. They also decorated the PCz moiety with large steric carbazole-substituted fluorene derivatives (**76–78**) to study the influences of subtle modulations on the bulkiness and stiffness of fluorene derivatives (9,9-dimethyl-9*H*-fluorene, 9,9-diphenyl-9*H*-fluorene, and 9,9′-spirobi[fluorene]) on the PL and EL properties of AIDF materials.[88] The results reveal that fluorene derivatives can effectively inhibit intermolecular interactions. On the other hand, the distorted and large steric conformation of the 9,9′-spirobi[fluorene] segment in **78** significantly decreases the electron mobility compared with the others (**76** and **77**). Eventually, the **78**-based nondoped device exhibits a much lower maximum EQE of 3.3% than the others (maximum EQEs of 19.0% and 18.5% for the **76**- and **77**-based devices, respectively).

To improve the solubility of AIDF emitters for solution-processed nondoped OLEDs, Qi *et al.*[89] exploited propeller-like dendritic luminogen **79** by connecting the central triphenylamine (TPA) unit with circumambient AIDF emitter (BP-PXZ derivative) arms. The branched alkyl chains in the Cz unit are beneficial for increasing the free volumes, which are important for improving the film-forming ability and preparing pinhole-free uniform films during the solution process. Using **79** as the nondoped EML in a solution-processed OLED with a device structure of ITO/PEDOT:PSS (40 nm)/**79** (40 nm)/TPBi (30 nm)/Cs_2CO_3 (2 nm)/Al (100 nm) realizes green emission with a peak at 529 nm and a maximum EQE of 12.1%.

Su *et al.*[90] reported two unsymmetrical D–A–A′-type AIDF emitters **80** and **81** by using PXZ, BP, and CN-substituted 3-phenyl-3,8*a*-dihydroimidazo[1,2-*a*]pyridine as the D, A, and A′ moieties, respectively. The introduction of strong electron-withdrawing CN groups can effectively redshift the emission to the long wavelength region. Therefore, the **80**- and **81**-based nondoped devices show ideal orange-red to red emissions with peaks at 592 and 610 nm, CIE coordinates of (0.54, 0.45) and (0.57, 0.42), and maximum EQEs of 4.9% and 3.7%, respectively.

Yasuda *et al.*[91] attempted to improve the IQE of BP-based AIDF emitters by increasing the rigidity of the BP unit. Compared with precursor **82**, fixing the BP unit with an oxygen bridge (xanthone (XT)) in **83** can effectively restrict the non-radiative process of the A moiety. Therefore, the **83** amorphous neat film exhibited a higher PLQY value of 0.53 than the 0.31 for **82**. They further clarified the actual mechanism of concentration quenching of TADF emitters by replacing the PTZ unit in **83** with rigid and steric 1,3,6,8-tetramethylcarbazole (MCz), 9,9-diphenylacridan (DPAc), spiro[acridan-9,9′-xanthene] (SXAc), and spiro[acridan-9,9′-fluorene] (SFAc) groups (**84–87**).[46] As shown in Fig. 7, they first revealed that the concentration quenching of TADF molecules was dominated by electron-exchange interactions for triplet excitons, and the inhibited intermolecular electron-exchange interactions in their condensed solid-states were the key to exploiting efficient TADF emitters for nondoped OLEDs.

By using XT as the A group, Tang *et al.*[92] also reported two D–A–D-type robust AIDF emitters **88** and **89**. Owing to the AIE character and well-restricted intermolecular interactions, both emitters show small ΔE_{ST}s of 0.025 and 0.024 eV, and excellent PLQYs of 0.96 and 0.94 in neat films, guaranteeing high-performance nondoped devices. Therefore, the **88**- and **89**-based nondoped devices emit intense green and sky-blue light with maximum EQEs of approximately 21.0%. Moreover, the **88**-based device displays outstanding efficiency stability with no efficiency roll-off (~0%) when the luminance increases to 1000 cd m^{-2}, which can be ascribed to the high and balanced hole and electron mobilities. However, compared with the

© 2022 The Author(s). Published by the Royal Society of Chemistry

Open Access Article. Published on 22 febbraio 2022. Downloaded on 08/05/2026 07:17:27.
This article is licensed under a Creative Commons Attribution-NonCommercial 3.0 Unported Licence.

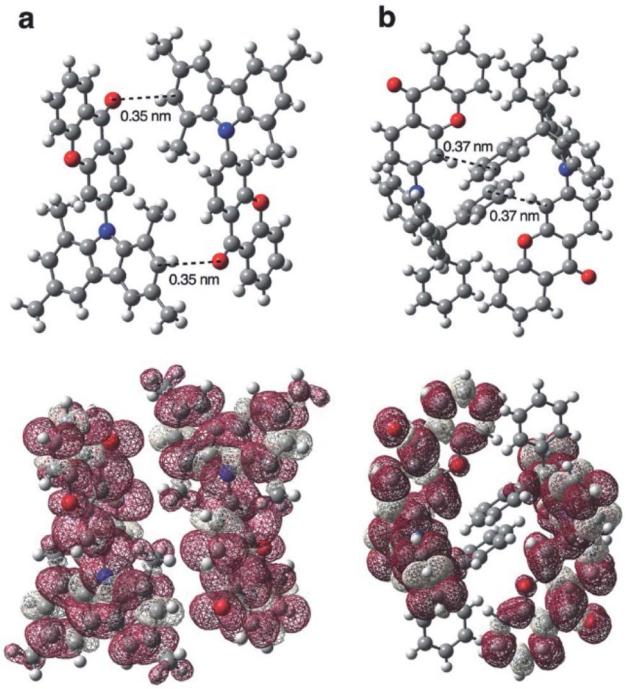

Fig. 7 Calculated spin-density distributions of the lowest-excited triplet states of (a) **84** and (b) **86** in the solid-state geometry determined by single-crystal X-ray analysis. Reproduced from ref. 46 with permission. Copyright 2016 Wiley-VCH.

performance of optimized doped devices (maximum EQEs of 25.0% and 27.0% for **88** and **89**, respectively), the efficiencies of nondoped devices are still less satisfactory, which can be reasonably ascribed to the unprotected electron-rich XT moiety. These results further indicate that both D and A moieties should be well shielded to suppress potential intermolecular packing-induced exciton quenching.

Wang *et al.*[93] reported a special ultrathin EML with a quantum well (QW) structure by using a previously reported TADF emitter **90**. The QW structure can effectively confine the charge carriers and excitons, affording high-efficiency and low-efficiency roll-off. A maximum EQE of 22.6% was achieved for the **90**-based nondoped device with seven quantum wells without any light outcoupling enhancement. However, the device shows severe efficiency roll-off at high luminance, maintaining only a small EQE of ~4.0% at a luminance of 1000 cd m^{-2}.

Conformational status is a fundamental issue for organic molecules to determine their overall properties. Wang *et al.*[94] developed TADF emitter **91** with dual stable conformations at the ground state. Both theoretical and physical tests show that the QE conformer with TADF characteristics plays a dominant role at the ground state, guaranteeing effective utilization of the excitons. Therefore, the **91**-based yellow nondoped device realizes a maximum EQE of 17.1%, current efficiency (CE) of 50.5 cd A^{-1}, and power efficiency (PE) of 60.0 lm W^{-1}.

To exploit efficient BP-based blue TADF emitters for nondoped OLEDs, Yasuda *et al.* reported a series of TADF emitters (**92–94**) combining isobenzofuranone (BF) or chromone (CM) as new A units with SXAc-based D units.[95] These materials realize bright blue TADF emissions centered at approximately 460–485 nm, with high PLQYs (0.53–0.78) and short τ_ds (2.8–3.8 μs).

TADF emitters with AIE features are hot candidates for nondoped devices, as they are highly emissive in the solid-state upon photoexcitation. Nevertheless, not every AIDF emitter in the past had guaranteed decent efficiencies in nondoped devices, indicating that the AIE character alone does not necessarily afford ideal nondoped TADF emitters. As shown in Fig. 8, our group designed three AIDF emitters **95–97** to investigate the critical molecular design rules.[96] The two new emitters (**96** and **97**) both retain the electron-donating and electron-withdrawing cores, as in reference compound **95**. The BP and

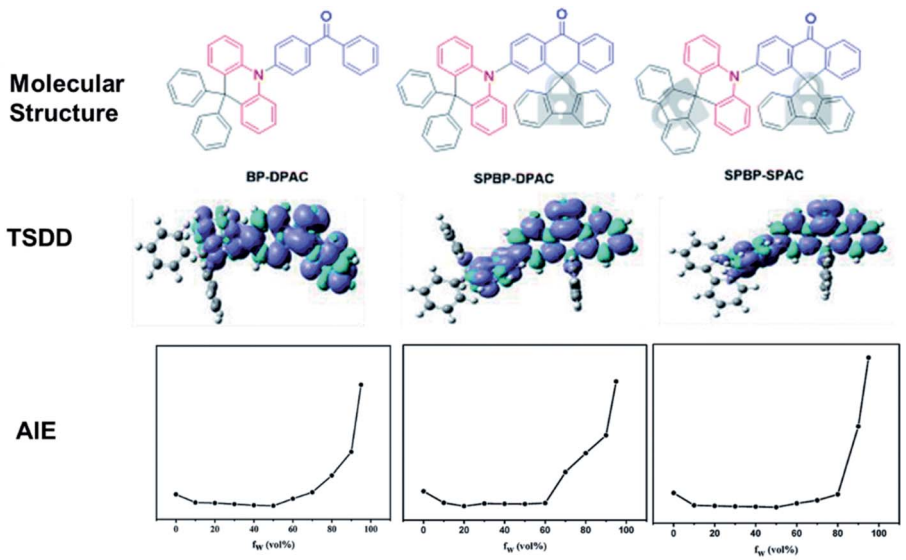

Fig. 8 Molecular structures, calculated triplet spin density distribution (TSDD) of the lowest-excited triplet states, and PL intensity *versus* different water fractions (f_w) of **95–97**. Reproduced from ref. 96 with permission. Copyright 2020 the Royal Society of Chemistry.

Open Access Article. Published on 22 febbraio 2022. Downloaded on 08/05/2026 07:17:27.
This article is licensed under a Creative Commons Attribution-NonCommercial 3.0 Unported Licence.

DPAc moieties were locked *via* a rigid fluorene group. Detailed physical measurements prove that these three compounds have similar energy levels as well as characteristics of AIE and TADF, while in neat films, **96** and **97** exhibit significantly higher exciton utilization in PL and EL processes, which can be ascribed to rigid steric fluorenes hindering intermolecular triplet–triplet interactions. Therefore, the nondoped OLEDs based on **96** and **97** display excellent maximum EQEs of 22.8% and 21.3%, respectively, which are evidently higher than that of the **95**-based OLED (12.9%). All these results demonstrate a feasible strategy of molecular modification to improve the nondoped EL performance of practical AIDF molecule candidates.

You *et al.*[97] designed a brand-new A moiety of heptagonal diimide (*N*-(4-(*tert*-butyl)phenyl)-1,1′-biphenyl-2,2′-dicarboximide (BPI)) and synthesized a D–A–D-type TADF emitter **98**. The rigidity of BPI can restrict excessive intramolecular rotation, thus enhancing k_r, while moderate rotatability can inhibit close intermolecular π–π packing, reducing exciton quenching in the aggregated state. Therefore, the corresponding nondoped device demonstrates a stable green emission with an emission peak at 511 nm and CIE coordinates of (0.25, 0.51). Moreover, the device achieves a maximum EQE of 24.7% with a small efficiency roll-off. Takano *et al.*[98] also applied phthalimide-based TADF emitter **99** to construct self-host cellulose derivatives for solution-processed nondoped OLEDs.

3.3. Sulfone-substituted aromatics as acceptors

Sulfone-substituted aromatics, such as diphenyl sulfoxide (DPS) and derivatives, have been widely used to construct TADF emitters due to their suitable electron-withdrawing abilities and limited molecular conjugations. The molecular structures of sulfone-based TADF emitters are shown in Fig. 9, and the corresponding key parameters of the nondoped devices are summarized in Table 3. By replacing the BP group in D–A–D-type TADF emitter **36** with a DPS moiety, Adachi *et al.*[72] also reported a novel efficient blue TADF emitter **100**. The methyl groups on the DMAC unit can effectively inhibit the intermolecular interactions; thus, the performances of the **100**-based devices are nearly concentration-independent. Moreover, in the neat film, **100** displays an even higher PLQY (0.88) than that of the doped film (0.80). To further lower the ΔE_{ST} and accelerate the RISC process, Guo *et al.*[99] designed a novel AIDF emitter **101** with a highly twisted zigzag molecular configuration. Compared with the *para*-positioned control compound **100**, connecting the DPS and DMAC units with a *meta*-position in **101** can effectively decrease the ΔE_{ST} and accelerate the RISC process. Therefore, the **101**-based pristine film exhibits a smaller ΔE_{ST} value of 0.02 eV, and the OLED exhibits a higher maximum EQE of 14.0% than those of **100** (a ΔE_{ST} of 0.18 eV and a maximum EQE of 11.2%).

Lee *et al.*[100] also designed DPS-based asymmetric and symmetric AIDF emitters **102** and **103** to investigate the relationship between molecular configuration and device performance. Since butterfly shaped PTZ groups induce conformational isomerizations,[101] PXZ-based asymmetric AIDF emitter **102** thus exhibits superior nondoped device performance with a maximum EQE of 17.0%.

To exploit DPS-based TADF emitters for solution-processed nondoped OLEDs, Yang *et al.*[102] proposed a multicarbazole

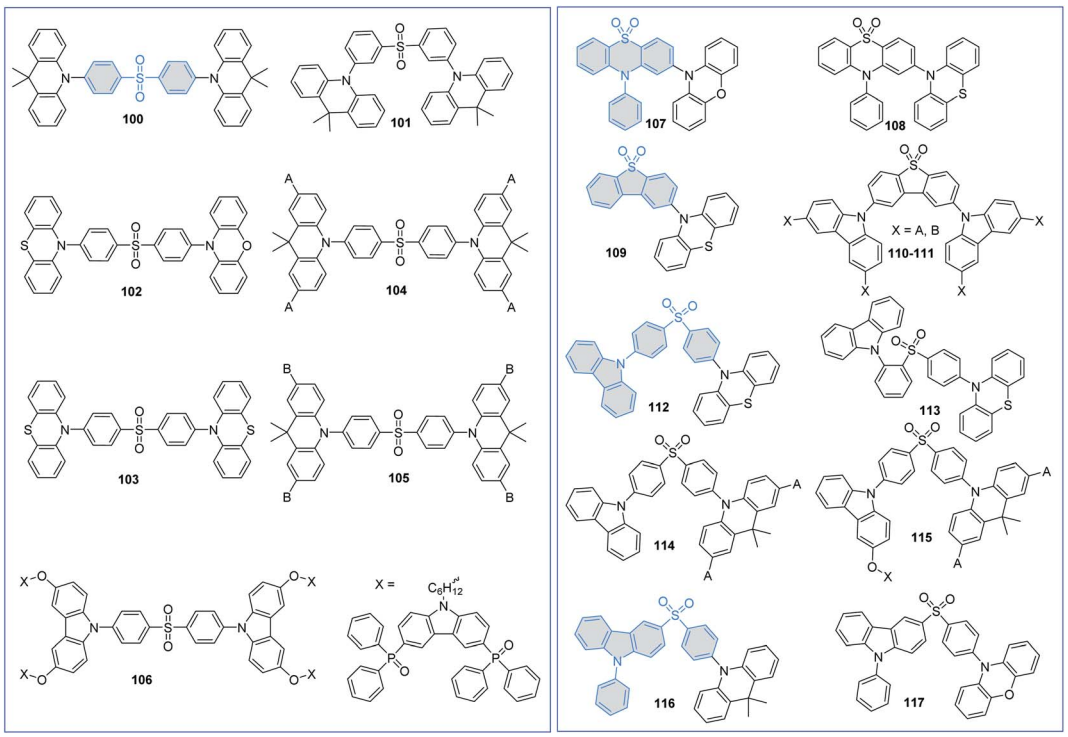

Fig. 9 Molecular structures of sulfone-based TADF emitters for nondoped OLEDs.

© 2022 The Author(s). Published by the Royal Society of Chemistry

Open Access Article. Published on 22 febbraio 2022. Downloaded on 08/05/2026 07:17:27.
This article is licensed under a Creative Commons Attribution-NonCommercial 3.0 Unported Licence.

Table 3 PL and EL properties of sulfone-based TADF emitters in nondoped films

	PL			EL						
						CE/PE/EQE [cd A^{-1}/lm W^{-1}/%]				
	PLQY	τ_p [ns]	τ_d [μs]	Peak [nm]	V_{on}[a] [V]	Maximum	@10^3 cd m^{-2}	Roll-off[b] [%]	CIE (x,y)	Ref.
100	0.88	—	—	480	4.3	—/—/19.5	—/—/14.6	25.1	(0.16, 0.29)	72
101	0.72	57.9	4.3	488	3.1	31.7/28.4/14.0	—	—	(0.18, 0.32)	99
102	—	—	—	~528	3.0	—/—/17.0	—/—/14.8	12.9	—	100
103	—	—	—	—	3.0	—/—/~14.0	—/—/~5.0	64.3	—	
104	0.68	—	—	502	3.6	30.6/24.0/12.2	11.3/5.1/4.5	63.1	(0.22, 0.44)	102
105	0.48	—	—	478	5.2	3.8/2.0/2.2	—	—	(0.18, 0.27)	
106	0.61	—	—	480	5.4	12.6/—/7.3	—	—	(0.18, 0.30)	103
107	0.62	16.1	2.5	504	4.3	44.9/32.0/16.4	—	—	(0.27, 0.50)	104
108	0.21	26.0	1870	510	3.4	9.2/8.3/3.3	0.8/0.2/0.3	90.9	(0.29, 0.49)	94
109	—	—	—	—	8.1	6.1/2.3/3.1	—	—	—	105
110	0.57	34.8	14.2	508	4.5	15.8/9.9/6.1	—	—	—	106
111	0.31	85.3	8.3	522	4.6	8.3/4.7/3.3	—	—	—	
112	0.97	6.3	62.2	518	3.5	61.2/38.4/20.7	—/—/10.0	51.7	—	107
113	0.92	4.4	19.1	524	4.1	82.3/51.8/28.7	—/—/2.8	90.2	—	
114	0.88	34.0	1.5	498	3.1	62.0/51.6/23.3	—	—	(0.23, 0.42)	108
115	0.96	22.0	1.4	500	3.0	65.9/59.2/24.0	—	—	(0.24, 0.45)	
116	0.65	7.7	2.4	484	2.9	17.0/15.7/9.1	—	—	(0.16, 0.28)	109
117	0.52	4.0	1.0	508	2.5	52.6/62.5/17.9	—	—	(0.28, 0.52)	

[a] Turn-on voltage at a luminance of 1 cd m^{-2}. [b] $EQE_{roll\text{-}off} = (EQE_{max} - EQE_{1000})/EQE_{max}$.

encapsulation strategy. By introducing carbazole dendrons (*t*BuCz and *t*BuCz2) into TADF emissive core **100**, two novel solution-processable DPS-based dendrimers **104** and **105** were synthesized. Multicarbazole encapsulation can not only improve the solubility but also minimize the concentration quenching effect, consequently reducing the quenching efficiency in OLEDs. Meanwhile, compared with *t*BuCz-decorated **104**, applying large steric *t*BuCz2 as the encapsulation group can significantly lower carrier transport. Thus, the **105**-based nondoped device exhibits a higher V_{on} of 5.2 V and a lower maximum EQE of 2.2% than those of **104** (a V_{on} of 3.6 V and a maximum EQE of 12.2%).

Sun *et al.*[103] also exploited a self-host dendrimer **106** for solution-processed nondoped OLEDs, in which the bipolar (9*H*-carbazole-3,6-diyl)bis(diphenylphosphine oxide) moiety was introduced through a long alkyl chain to ensure balanced carrier transport. Peripheral bipolar dendrons can not only improve the morphological stability but also restrain the concentration quenching effect of the TADF emissive core bis[4-(3,6-dimethoxycarbazole)phenyl] sulfone (DMOC-DPS). Therefore, the spin-coated OLED featuring **106** achieves a maximum EQE of 7.3%.

To further reduce exciton annihilation, increasing the rigidity of the DPS group is a feasible method. By oxidizing the sulfur atom in the PTZ unit, Wang *et al.*[104] designed a novel A moiety named 10-phenyl-10*H*-phenothiazine-5,5-dioxide (2PTO). Further introducing rigid and planar PXZ units as the D moiety, green AIDF emitter **107** with a highly stereoscopic structure was thus synthesized. The **107**-based nondoped device exhibits a high efficiency with a maximum EQE of 16.4%, which is comparable with that of the corresponding doped counterpart. They also tried to replace the planar PXZ unit (**107**) with the butterfly shaped PTZ unit (**108**).[94] Owing to the stable QA conformer at the ground state, **108** shows conventional fluorescence emission. Therefore, compared with the BP-based analog **91**, **108** exhibits a lower PLQY and poorer device performance. These results indicate that molecular conformational distributions will significantly influence device performance and need more in-depth research.

Dias *et al.*[105] designed TADF emitter **109** by using butterfly shaped PTZ and rigid dibenzothiophene-*S*,*S*-dioxide (DBTO2) as the D and A moieties, respectively. The presence of a suitable ^{3}LE (2.66 eV of the DBTO2 group) close to the CT manifold (2.61 eV of **109**) is expected to accelerate the RISC process and facilitate the utilization of triplet excitons. Nevertheless, compared with the doped ones (a maximum EQE of up to 22.0%), its nondoped device only exhibits a very poor performance with a maximum EQE of only 3.1%. This is mainly attributed to the low charge mobilities. By utilizing the dendronization strategy on precursor molecule 2,8-bis(3,6-di-*tert*-butyl-9*H*-carbazol-9-yl)dibenzo[*b*,*d*]thiophene-5,5-dioxide (*t*BuCz-DBTO2), Yang *et al.*[106] designed a series of DBTO2-based dendrimers **110–111** for solution-processed nondoped OLEDs. Encapsulation of the parent *t*BuCz-DBTO2 TADF core with a soluble *t*BuCz moiety can not only enhance the morphological stabilities but also effectively lower the ΔE_{ST}s by decreasing the overlap of the FMOs. As a result, their solution-processed nondoped devices exhibit gradually redshifted EL emissions (456, 508 and 522 nm for *t*BuCz-DBTO2, **110** and **111**, respectively) with increasing generation number of dendrimers. In addition, the **110**-based device displays the best EL performance with a maximum EQE of 6.1%, which is nearly double that of the **111**-

Open Access Article. Published on 22 febbraio 2022. Downloaded on 08/05/2026 07:17:27.
This article is licensed under a Creative Commons Attribution-NonCommercial 3.0 Unported Licence.

based device (3.3%) and more than 20-fold higher than that of the *t*BuCz-DBTO2-based device (0.3%).

To regulate the molecular packing and bipolar carrier transport more conveniently, asymmetric DPS-based TADF emitters have been extensively investigated. Chi *et al.*[107] designed two asymmetric D–A–D′-type AIDF emitters **112** and **113** by using PTZ, DPS, and Cz as the D, A, and D′ moieties, respectively. Further introducing an *ortho*-positioned Cz unit in **113** guarantees the coexistence of intramolecular electrostatic attractions and through-space CT, leading to reduced structural vibrations, suppressed nonradiative decay, and rapid radiative decay to avoid excited state energy loss. As a result, the **113**-based nondoped device exhibits a state-of-the-art performance with a maximum EQE of 28.7%. However, at 1000 cd m^{-2}, the EQE of this nondoped device dramatically declined to approximately 2.8%. Such a serious efficiency roll-off can be ascribed to the unbalanced carrier mobilities.

Yan *et al.* proposed that the poor device performance of DPS-based fully conjugated (**104**) or fully nonconjugated (**106**) structures can be attributed to the unwanted degenerate excited states generated by multiple identical dendrons. To suppress the formation of degenerate excited states, two new asymmetrical "half-dendronized" (**114**) and "half-dendronized–half-encapsulated" (**115**) emitters have been designed and synthesized.[108] Both emitters show distinct AIDF properties, which minimize the exciton quenching in aggregated states, and consequently reduce their efficiency roll-off in their nondoped devices. Moreover, the asymmetric molecular structures successfully limit the unwanted degenerate excited states, favoring the TADF characteristics. As a result, the solution-processed nondoped devices using **114** and **115** as the pure EMLs achieved maximum EQEs of 23.3 and 24.0%, respectively.

Wang *et al.* also reported two asymmetric AIDF emitters **116** and **117** by using DMAC/PXZ, DPS, and PCz as the D, A, and D′ moieties, respectively.[109] Introducing the PCz moiety can effectively restrain the intermolecular interactions in the aggregated states. Therefore, both emitters exhibit typical AIDF characteristics. Moreover, due to the obviously enhanced electron-donating ability of the PXZ unit, the **117** amorphous neat film exhibits a smaller ΔE_{ST} of 0.03 eV and shorter τ_d of 1.0 μs than **116** (ΔE_{ST} and τ_d of 0.07 eV and 2.4 μs, respectively). Therefore, the nondoped OLEDs obtained by using **116** and **117** as the pure EMLs achieve maximum EQEs of 17.9 and 9.1%, respectively.

3.4. Nitrogen-containing heterocycles as acceptors

Nitrogen-containing heterocycles, such as terpyridine, pyrimidine, quinoline, quinoxaline, triazine, and dibenzo[*a*,*c*]phenazine, have been widely used to exploit TADF emitters for nondoped OLEDs. Herein, we classify nitrogen-containing heterocycles based on their different electron-withdrawing abilities (exhibited in Fig. 10 and summarized in Table 4). To effectively restrict exciton quenching in the aggregated solid-state, we have proposed a novel strategy of exploiting high-performance nondoped electroluminescence by tuning intermolecular hydrogen bonding.[50] Three TADF isomers **118–120** were synthesized by using PXZ and *o*/*m*/*p*-terpyridine as the D and A moieties, respectively. As displayed in Fig. 11, suitable intermolecular hydrogen bonding (**119**) enables the formation of a 3D supramolecular framework, which can evidently restrict

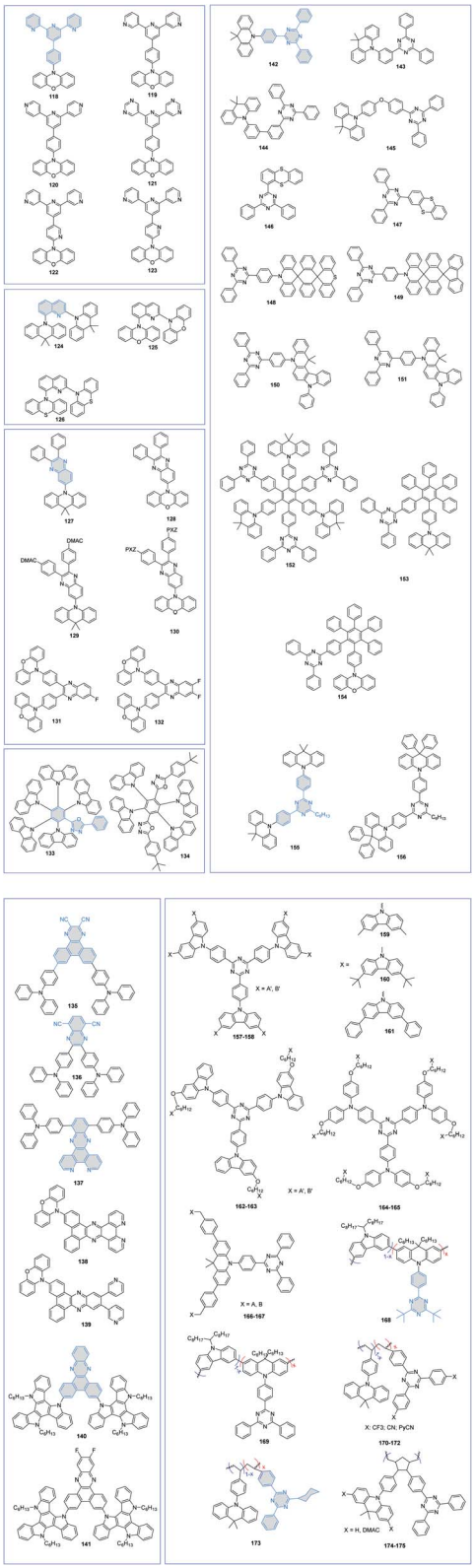

Fig. 10 Molecular structures of nitrogen-containing heterocycle-based TADF emitters for nondoped OLEDs.

© 2022 The Author(s). Published by the Royal Society of Chemistry

Open Access Article. Published on 22 febbraio 2022. Downloaded on 08/05/2026 07:17:27.
This article is licensed under a Creative Commons Attribution-NonCommercial 3.0 Unported Licence.

Table 4 PL and EL properties of nitrogen-containing heterocycle-based TADF emitters in nondoped films

	PL			EL						
						CE/PE/EQE [cd A^{-1}/lm W^{-1}/%]				
	PLQY	τ_p [ns]	τ_d [μs]	Peak [nm]	V_{on}[a] [V]	Maximum	@10^3 cd m^{-2}	Roll-off[b] [%]	CIE (x,y)	Ref.
118	0.52	14.4	4.4	528	—	24.7/20.3/8.2	23.6/17.2/7.6	7.3	(0.33, 0.56)	50
119	0.82	19.1	7.0	532	—	79.8/83.8/23.6	74.1/72.7/21.9	7.2	(0.34, 0.56)	
120	0.64	23.8	5.2	540	—	50.4/52.8/16.4	43.5/34.1/14.1	14.0	(0.38, 0.55)	
121	0.90	24.4	1.1	560	—	70.0/90.1/21.8	64.5/60.0/20.1	7.8	(0.44, 0.54)	111
122	0.80	13.1	17.3	548	2.6	84.1/96.5/25.4	78.4/71.9/23.6	7.1	(0.40, 0.56)	49
123	0.47	19.2	6.7	560	2.6	44.5/46.2/14.6	41.3/36.2/13.6	6.8	(0.45, 0.53)	
124	0.80	18.5	16.0	534	3.0	58.1/57.0/17.4	—/—/∼7.2	58.6	—	116
125	0.58	57.7	2.8	570	3.2	42.4/31.6/14.9	—/—/∼12.8	14.1	—	
126	0.36	22.3	3.3	568	3.2	36.8/30.4/13.1	—/—/∼7.4	43.5	—	
127	0.74	23.0	8.3	544	2.8	35.4/32.7/10.1	21.2/10.7/6.0	40.6	(0.39, 0.58)	117
128	0.73	32.0	2.4	608	2.4	10.5/12.0/5.6	9.8//5.2/5.2	7.1	(0.56, 0.43)	
129	0.84	26.0	6.5	548	2.6	41.2/45.4/12.0	28.5/17.6/8.3	30.8	(0.40, 0.57)	
130	0.76	29.0	1.9	616	2.8	7.5/6.2/5.3	6.2/2.9/4.4	17.0	(0.60, 0.40)	
131	0.73	57.0	3.4	584	3.4	24.3/22.5/10.1	14.2/6.3/6.0	40.6	—	118
132	0.74	68.0	3.3	588	3.2	21.0/20.6/9.8	9.8/4.2/4.7	52.0	—	
133	—	—	—	492	2.6	9.9/12.0/3.6	6.1/2.9/2.2	38.9	(0.23, 0.43)	119
134	0.71	—	—	546	2.9	—/—/20.9	61.6/41.5/18.0	13.9	—	120
135	0.14	20.8	0.8	710	4.0	0.24/0.19/2.1	—	—	(0.70, 0.29)	121
136	0.31	12.2	13.2	700	3.2	0.80/0.78/4.6	—/—/1.3	71.7	(0.70, 0.30)	37
137	0.87	10.2	5.0	652	7.0	8.1/3.6/12.3	7.0/1.9/10.7	13.0	(0.67, 0.33)	122
138	0.16	—	—	656	—	1.3/0.8/2.2	—	—	(0.65, 0.35)	124
139	0.33	—	—	680	—	2.8/2.3/5.2	—	—	(0.68, 0.32)	
140	—	—	—	626	3.0	7.3/7.6/5.6	2.9/1.5/2.2	60.7	(0.61, 0.38)	125
141	—	—	—	641	3.0	2.5/2.6/2.9	0.8/0.3/0.9	69.0	(0.64, 0.35)	
142	0.83	—	—	∼515	∼3.0	61.1/45.7/20.0	—	—	—	126
143	0.52	93	5.8	524	3.4	15.0/5.8/5.7	—	—	(0.33, 0.54)	128
144	0.69	59	1.8	—	3.6	45.1/37.3/18.7	—	—	(0.24, 0.49)	
145	0.47	—	—	504	3.0	39.3/37.0/14.7	30.0/21.2/11.3	23.1	(0.22, 0.45)	51
146	0.79	1.3	229.8	524	3.3	67.4/62.3/20.3	—	—	(0.31, 0.57)	129
147	0.44	11.1	—	498	3.5	10.3/9.5/3.8	—	—	(0.20, 0.44)	
148	0.70	21.8	2.8	∼478	3.3	41.1/35.8/20.0	21.9/14.9/10.6	47.0	(0.16, 0.30)	130
149	0.64	22.3	3.2	∼486	3.3	39.0/33.5/16.5	22.8/15.8/9.7	41.2	(0.18, 0.34)	
150	0.42	55.0	0.8	576	3.4	18.0/15.5/7.3	14.6/6.3/5.9	19.2	(0.50, 0.49)	131
151	0.67	81.0	0.6	548	3.1	45.2/40.0/14.1	41.2/26.1/12.8	9.2	(0.42, 0.55)	
152	0.20	—	—	520	3.4	11.4/—/3.5	9.5/—/3.0	14.3	(0.30, 0.54)	132
153	0.52	48.4	4.7	521	3.1	21.4/17.6/6.5	19.9/13.0/6.0	7.7	(0.28, 0.58)	133
154	0.62	41.6	2.1	544	2.5	41.2/44.9/12.7	40.1/31.5/12.3	3.1	(0.39, 0.57)	
155	0.36	35.9	3.5	494	3.1	33.6/32.6/12.8	22.9/11.2/8.7	32.0	(0.24, 0.47)	134
156	0.85	19.1	2.4	467	3.1	28.6/28.4/15.8	7.9/3.4/4.4	72.2	(0.18, 0.27)	
157	0.52	—	—	∼503	3.3	—/—/2.4	—/—/∼1.4	41.7	(0.25, 0.49)	135
158	0.31	—	—	∼510	3.5	—/—/3.4	—/—/∼1.4	58.8	(0.27, 0.49)	
159	0.40	15.7	3.3	510	3.0	26.5/21.5/9.4	—/—/7.1	24.4	—	136
160	0.44	13.3	5.3	510	3.5	25.4/16.1/9.5	—/—/7.3	23.2	—	
161	0.49	14.5	1.9	510	3.2	23.1/17.3/8.2	—/—/6.0	26.8	—	
162	0.58	—	—	490	4.0	20.0/—/6.5	∼4.9	24.6	(0.24, 0.51)	137
163	0.76	—	—	487	3.6	30.5/—/10.1	29.0/—/∼9.0	10.9	(0.24, 0.51)	
164	0.56	—	0.5	490	4.0	20.0/—/6.5	—	—	(0.24, 0.51)	138
165	0.77	—	0.8	487	3.6	30.5/—/10.1	29.0/—/—	—	(0.24, 0.51)	
166	0.69	21.7	2.9	520	4.0	30.8/24.2/9.5	—	—	(0.32, 0.57)	139
167	0.56	16.1	25.2	496	4.5	20.7/14.5/8.1	—	—	(0.22, 0.43)	
168	0.90	11.1	2.5	∼530	2.6	—/48.5/16.9	—/34.3/15.6	7.7	(0.35, 0.54)	140
169	0.89	27.9	1.1	∼545	2.6	48.7/50.5/15.5	45.9/34.3/14.5	6.4	(0.41, 0.55)	141
170	0.74	44.0	2.0	525	3.0	50.3/—/16.2	40.2/—/13.0	19.8	(0.34, 0.55)	142
171	0.34	53.0	0.8	568	3.2	21.1/—/7.8	11.9/—/4.4	43.6	(0.46, 0.50)	
172	0.06	44.0	0.9	616	4.0	1.7/—/1.0	0.4/—/0.3	70.0	(0.57, 0.41)	
173	0.29	66.0	0.4	455	3.2	10.6/—/7.1	5.8/—/3.9	45.1	(0.17, 0.17)	
174	0.56	44.8	2.4	469	3.2	26.1/—/12.9	24.8/—/12.3	4.6	(0.19, 0.26)	143
175	0.81	45.4	2.5	479	2.8	42.7/—/18.8	36.4/—/16.1	14.4	(0.20, 0.31)	

[a] Turn-on voltage at a luminance of 1 cd m^{-2}. [b] $EQE_{roll\text{-}off} = (EQE_{max} - EQE_{1000})/EQE_{max}$.

Open Access Article. Published on 22 febbraio 2022. Downloaded on 08/05/2026 07:17:27.
This article is licensed under a Creative Commons Attribution-NonCommercial 3.0 Unported Licence.

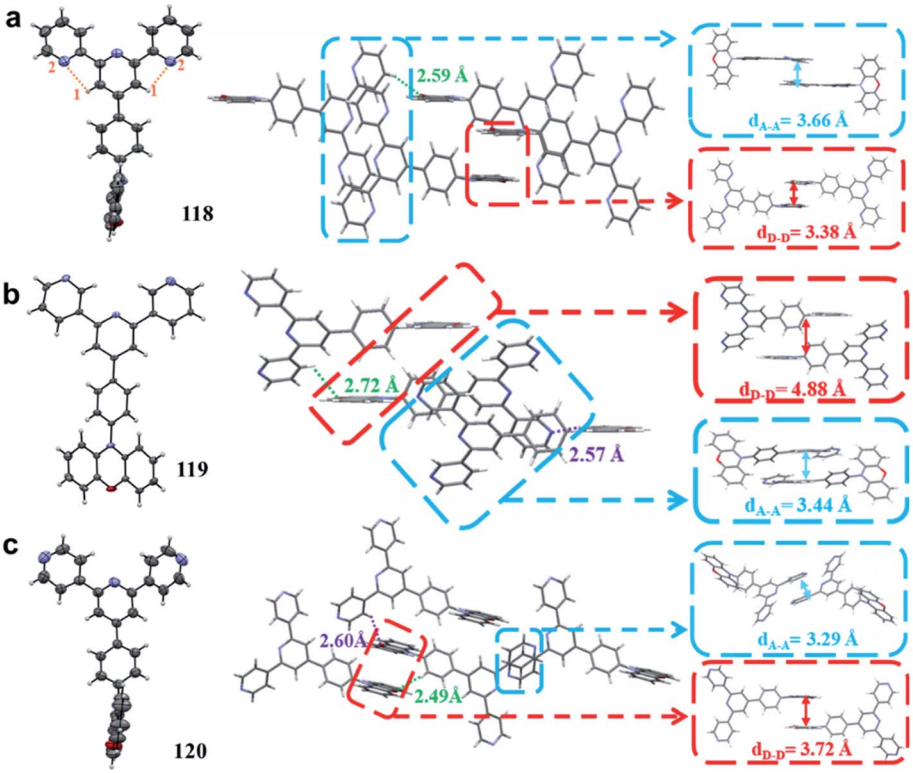

Fig. 11 Thermal ellipsoid drawings at the 50% probability level and intermolecular geometries of (a) **118**, (b) **119**, and (c) **120** in the single crystals determined by X-ray analysis. Reproduced from ref. 50 with permission. Copyright 2020 the Royal Society of Chemistry.

the nonradiative process and suppress triplet exciton quenching caused by π–π packing of triplets. Moreover, such a 3D supramolecular structure also favors horizontal molecular orientations, which can evidently increase the outcoupling efficiency and benefit realization of high device performance.[110] Therefore, the **119**-based nondoped device exhibits state-of-the-art performance with a maximum EQE of 23.6% with only 7.2% roll-off at 1000 cd m^{-2}. Moreover, it is the first report that the performance of a TADF-based nondoped device can evidently surpass that of its corresponding optimized doped counterpart (maximum EQE = 16.3%), indicating that the intermolecular hydrogen bonding mechanism can not only provide a new pathway for designing TADF emitters for high-performance nondoped devices, but also has great potential in other solid-state luminescence applications. By replacing the peripheral pyridine ring in **119** with a more electron-withdrawing pyrimidine unit, we further synthesized a novel TADF emitter **121**.[111] Unlike the formation of a 3D framework in **119**, the X-ray data show that a 1D chain can be observed in **121**. Such a linear chain structure can effectively keep the electron-rich PXZ cores in neighboring molecules apart from each other such that triplet-related exciton quenching can be well suppressed. In addition, it also improves the balance of carrier mobilities and the optical outcoupling from the EML. With these merits, OLEDs using **121** as a dopant emitter, from 10 to 100 wt%, can maintain high EQEs of over 20%. More importantly, the nondoped OLED shows yellow emission and an excellent maximum EQE of 21.8% with a small efficiency roll-off, which is even comparable with that of state-of-the-art yellow OLEDs. These results provide new insight into the role of hydrogen bonding in molecular packing and its subsequent influences on the performance of OLEDs.

Conformational status is a fundamental issue for TADF emitters to determine their overall properties. Recently, TADF emitters with dual conformations have been widely studied.[112–115] However, unlike the detailed investigations between conformational isomerization and excited-state properties in the dilute solution state, their influences in the amorphous solid-state are far from clear due to the lack of a suitable quantitative analysis method. By using temperature-dependent time-resolved photoluminescence spectroscopy, we quantitatively measured the conformational populations for the first time.[49] The populations of the quasi-axial (QA) and quasi-equatorial (QE) forms of newly designed TADF emitter **122** in the disordered solid-state were thus measured to be 86 and 14%, respectively. Interestingly, this "compositionally" pure film actually behaves as a film with a dopant (QE form) in a matrix (QA form). In terms of the conformational distribution aspect, we further propose a new concept of "self-doping" for realizing high-efficiency nondoped OLEDs (Fig. 12). The "self-doping" OLED realizes superior device performance with a maximum EQE of 25.4% and neglectable efficiency roll-off. This is similar to those in state-of-the-art OLEDs with "dopant-in-host" systems. On the other hand, as the emitting film employs only one compound, the issues of higher

© 2022 The Author(s). Published by the Royal Society of Chemistry

Open Access Article. Published on 22 febbraio 2022. Downloaded on 08/05/2026 07:17:27.
This article is licensed under a Creative Commons Attribution-NonCommercial 3.0 Unported Licence.

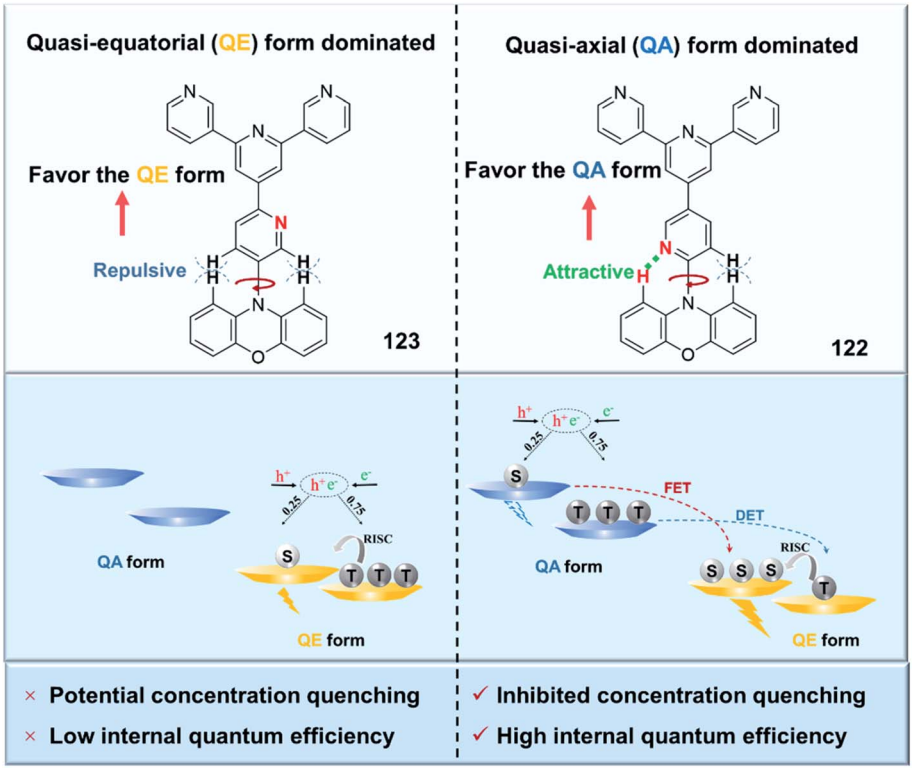

Fig. 12 Molecular structures of **122** and **123** and a schematic illustrating the distribution of the conformations at the ground state and corresponding energy transfer at excited states.

manufacturing cost and potential dopant segregation associated with "dopant-in-host" systems can be effectively avoided.

Chen *et al.*[116] designed and synthesized three AIDF emitters **124–126** by using the quinoline unit as a new A group. Owing to the highly twisted D–A molecular framework, all three quinoline-based emitters display small ΔE_{ST} values (~0.04 eV), good photoluminescence, and AIDF properties. Meanwhile, the steric DMAC group in **124** can effectively retain the intermolecular mutual interactions and favor the utilization of the excitons. Therefore, the **124**-based nondoped device displays a superior performance with a maximum EQE of 17.4%, much higher than that of the others (maximum EQEs of 14.9% and 13.1% for **125** and **126**, respectively). To further exploit quinoline-based emitters for high-performance red/orange nondoped OLEDs, Yang *et al.*[117] designed a series of AIDF emitters **127–130** by simultaneously modulating the D units and regulating the degree of ICT characteristics. They also decorated the quinoline unit with the fluorine atom (**131** and **132**).[118] Introducing the fluorine atom can not only slightly enhance the electron-withdrawing ability but also enrich the intermolecular electron coupling capability. The nondoped OLEDs obtained by using **131** and **132** as the EMLs achieve orange emission with EL peaks of 584 and 588 nm and maximum EQEs of 10.1% and 9.8%, respectively.

Tao *et al.*[119] modified the efficient sky-blue precursor 5CzBN by replacing the CN unit with a 1,3,4-oxadiazole (OXD) moiety (**133**). It exhibits bright light-blue emission, with a maximum EQE of 3.6% of the nondoped device. Moreover, it functions as a highly efficient host for green and yellow TADF OLEDs. Kippelen *et al.*[120] further modified the molecule by introducing two *t*Bu-substituted OXD moieties (**134**). Due to effectively restricted exciton quenching owing to the steric *t*Bu group, the **134** pristine neat film exhibits a high PLQY of 0.71. The corresponding nondoped OLED yields a maximum EQE of 20.9% and a high luminance of 120 000 cd m^{-2}.

By applying TPA and 2,3-dicyanopyrazino phenanthrene (DCPP) as the D and A moieties, respectively, Wang *et al.*[121] synthesized the first V-shaped TADF emitter **135** for near-infrared (NIR) nondoped OLEDs. A large and rigid π-conjugated DCPP moiety can effectively restrain the molecular vibration and rotational processes, while an electron-donating TPA moiety can not only offer excellent hole-transporting capability but also diminish exciton quenching in the aggregated state. Therefore, a small ΔE_{ST} and high k_r value can be simultaneously obtained, benefiting the utilization of electrogenerated excitons. The corresponding nondoped device realizes NIR emission with a peak at 710 nm and CIE coordinates of (0.70, 0.29). Xu *et al.*[37] also developed a novel NIR TADF emitter by using the CN-decorated quinoline unit as the A moiety (**136**). The **136**-based nondoped device realizes a maximum EQE of 4.6% with NIR emission at a peak of 700 nm.

By modulating the substitution position of the TPA unit from the *o*- to the *p*-position, Xu *et al.*[122] developed a novel "T-shaped" deep-red TADF emitter **137** by using the planar dipyridophenazine (DPPZ) moiety as the A. In comparison to the *o*-substituted precursor,[123] the rational spatial arrangement of D

Open Access Article. Published on 22 febbraio 2022. Downloaded on 08/05/2026 07:17:27.
This article is licensed under a Creative Commons Attribution-NonCommercial 3.0 Unported Licence.

and A groups in **137** can not only remarkably improve the carrier transport but also dramatically accelerate the rate of k_r by 90-fold without worsening the nonradiative transition process (k_{nr}^S) and amplify the thermodynamic advantage of RISC with a nearly unitary efficiency, giving rise to a PLQY as high as 0.87. Therefore, the corresponding nondoped device realizes a record high EQE of 12.3% for the maximum and 10.4% at 1000 cd m^{-2}. All these results demonstrate that it is important to obtain deep insight into the influence of the spatial arrangement of functional groups on the optoelectronic properties.

Based on the DCPP moiety, our group also designed two TADF emitters **138** and **139** to demonstrate the relationship between molecular rigidity and intermolecular packing.[124] Although the fused dibenzo[*a*,*c*]dipyrido[3,2-*h*:2′,3′-*j*]phenazine (BPPZ) moiety can effectively relieve the nonradiative process, a large planar molecular structure induces unavoidable intermolecular π–π interactions, which are detrimental to the performance of nondoped devices. The rotational pyridine unit in 2,3-di(pyridin-3-yl)dibenzo[*f*,*h*]quinoxaline (*m*DPBPZ) can provide suitable steric hindrance against intermolecular π–π packing. The **138**-based doped device realizes a remarkably high maximum EQE of 25.2%, while the **139**-based nondoped device shows a relatively high EQE of 5.2% with deep red/NIR emission at a peak of 680 nm.

Wang *et al.*[125] designed two AIDF emitters **140** and **141** by using rigid TAT and dibenzo[*a*,*c*]phenazine (DBPZ)/fluorine-decorated DBPZ as the D and A moieties, respectively. The large steric hindrance between planar TAT and DBPZ segments can not only restrain the overlap of the FMOs but also suppress aggregation-caused quenching. Therefore, both compounds possess TADF characteristics with small ΔE_{ST}s and AIE properties. The **140**- and **141**-based solution-processable nondoped OLEDs exhibit red and deep-red emissions (CIE coordinates of (0.61, 0.38) and (0.64, 0.35)) with maximum EQEs of 5.6 and 2.9%, respectively.

With three potential modification sites, the triazine (TRZ) group with highly electron-deficient properties is a suitable building block for constructing TADF emitters. By using DMAC/PXZ and TRZ as the D and A groups, respectively, Wu *et al.* designed two TADF emitters, PXZ-TRZ and **142**.[126] Compared with PXZ-TRZ, the DMAC unit in **142** can effectively restrict exciton quenching in the solid-state and guarantee that the **142** neat film realizes a high PLQY of 0.83. As a result, a highly efficient nondoped device with a maximum EQE of 20.0% is also realized. Kaji *et al.*[127] further applied **142** for solution-processed nondoped OLEDs. The peripheral phenyl units and large steric methyl units in the TRZ and DMAC moieties, respectively, can effectively suppress the intermolecular interactions. Therefore, the spin-coated **142** neat film displays a high PLQY of 0.84, which is almost identical to that of a vacuum vapour deposited neat film. Hong *et al.*[128] also connected the DMAC and TRZ units *via* a *meta*-position and synthesized two TADF emitters **143** and **144** with molecular structures of D–A and D–π–A, respectively. Compared with D–A-type molecule **143**, introducing the π group in **144** more efficiently benefits the formation of intermolecular exciplexes. Therefore, the **144**-based nondoped device exhibits a superior device performance with a maximum EQE of 18.7%, much higher than that of **143** (5.3%).

To relieve triplet exciton quenching in the aggregated solid-state, our group proposed a novel molecular model to develop TADF emitters radiating *via* the intermolecular CT transition for nondoped OLEDs.[51] As displayed in Fig. 2f, the DMAC and TRZ moieties were connected with a space-enough and conjugation-forbidden linkage (diphenyl ether linkage), which was called the D–spacer–A structure. Such a molecular structure can effectively suppress the intramolecular CT transition while forming an exciplex-type emitter *via* the intermolecular CT transition. Therefore, **145** exhibits local excited properties in a single-molecule state, as the D–spacer–A molecular backbone strongly suppresses the intramolecular CT transition. With increasing doping concentration, the intermolecular CT transition becomes significant, opening another effective radiation channel and resulting in TADF characteristics. The corresponding devices thus exhibit similar performance under various high doping ratios (40–100 wt%), and the nondoped device retains a high maximum EQE of 14.7%. These results prove that the intermolecular CT transition not only endows emitters with natural TADF but also helps to inhibit the undesired concentration quenching effect. Therefore, the D–spacer–A structure molecule could act as a novel candidate to develop TADF emitters with intermolecular CT transitions for efficient nondoped OLEDs.

At present, the majority of TADF emitters are based on largely twisted aromatic amine-based compounds. To broaden the choice of the D moieties, Su *et al.*[129] designed two TADF emitters **146** and **147** by using thianthrene (TE) and TRZ, respectively, as the D and A groups. Unlike only the existing π-conjugated CT channel in linear **147**, *ortho*-substituted **146** exhibits a twisted D–A backbone with coexistence through the bond and through spatial CT. As a result, the **146** amorphous neat film has a high PLQY of 0.79, which is much higher than that of **147** (0.44). Therefore, the **146**-based nondoped device produces a green emission with a maximum EQE of 20.6%, which is comparable to those of the reported aromatic amine-based counterparts. They also designed two novel tri-spiral units, 10*H*-dispiro[acridine-9,9′-anthracene-10′,9″-thioxanthene] (TspiroS) and 10*H*-di acridine-9,9′-anthracene-10′,9″-fluorene] (TspiroF), with long bar shapes for high-performance nondoped OLEDs.[130] By further integrating a strong TRZ acceptor moiety, two linear TADF emitters **148** and **149** were designed and synthesized. Compared with the nonspiral and dual-spiral acridine units, the elongation of the molecular backbone with a large nonconjugated fragment can unambiguously increase the distance between the adjacent luminophores and weaken the intermolecular interactions. Moreover, the long and linear molecular configurations favor the horizontal dipole ratio, which can significantly enhance the out-coupling efficiency of the device.[110] As a result, sky-blue nondoped OLEDs realize maximum EQEs of 20.0% and 16.5% for **148** and **149**, respectively.

Wang *et al.*[131] designed a novel indole-fused acridine D group donor (13,13-dimethyl-8-phenyl-8,13-dihydro-5*H*-indolo[3,2-*a*]acridine, 34AcCz). Then, two AIDF emitters **150** and **151** were

© 2022 The Author(s). Published by the Royal Society of Chemistry

Open Access Article. Published on 22 febbraio 2022. Downloaded on 08/05/2026 07:17:27.
This article is licensed under a Creative Commons Attribution-NonCommercial 3.0 Unported Licence.

designed and synthesized by using TRZ and 2,6-diphenylpyrimidine (PM), respectively, as the A moieties. Through systematic analysis of structure–property correlation, **151** was found to have a more prominent AIE characteristic with a higher PLQY. Thus, the **151**-based nondoped device exhibits a maximum EQE of 14.1%, double that of **150** (a maximum EQE of 7.3%).

Hexaarylbenzene (HAB) derivatives, in which six aromatic rings are arranged around the central phenyl ring with a propeller-shaped configuration, can be considered the desired model to carefully investigate the through-space CT process. Wang *et al.*[132] designed a novel AIDF emitter **152** with circularly arrayed DMAC and TRZ units in the periphery of the HAB core. Such a propeller-shaped molecular structure not only favors a reduced ΔE_{ST} but also facilitates k_r. Nevertheless, the corresponding solution-processed nondoped device can only realize poor device performance with a maximum EQE of 3.5%. Tang *et al.*[133] also decorated the HAB with DMAC/PXZ and TRZ units positioned in close proximity (**153** and **154**) to ensure that electron clouds of D and A exchange through spatial interactions. Due to the enhanced electron-donating ability of the PXZ unit, the **154** amorphous neat film shows a smaller ΔE_{ST} value of 0.02 eV than DMAC-based **153** (0.09 eV). Moreover, the AIE-active HAB moiety can effectively enlarge the intermolecular distance and relieve the ACQ effect. Therefore, the **154**-based nondoped device realizes a superior performance with a maximum EQE of 12.7% and a neglectable efficiency roll-off at high luminance.

Chang *et al.*[134] modified the TRZ unit with a long alkyl chain to inhibit unwanted intermolecular D–D/A–A-type π–π interactions and accordingly designed two D–A-type TADF emitters **155** and **156**. Owing to the nature of the electron-donating ability of the alkyl chain, the LUMO of the modified TRZ unit can be slightly weakened, generating blueshifted emission. Meanwhile, the crowded molecular architecture favors well-separated FMOs and benefits TADF properties. As a result, blue-emitting nondoped devices with **155** and **156** as the EMLs reveal satisfactory efficiencies of 12.8% and 15.8%, respectively.

Yamamoto *et al.*[135] first designed Cz-decorated TRZ-based TADF dendrimers **157** and **158** by decorating the precursor 2,4,6-tris(4-(9*H*-carbazol-9-yl)phenyl)-1,3,5-triazine (TCz-TRZ) for solution-processed nondoped OLEDs. Intermolecular interactions between the adjacent emissive cores decrease when the generation number of the Cz unit increases. The second-generation **158**-based solution-processable nondoped device exhibits a superior performance compared to **157**. Although device performance should be improved by careful optimization, more importantly, the recorded EQE value indicated that the dendrimer emitting layer can harvest triplet excitons. These TRZ-based dendrimers are the first high-molecular-weight TADF materials for solution-processable nondoped OLEDs. To realize fully solution-processed devices, they also tried to decorate precursor **157** by introducing methyl, *t*Bu, and phenyl groups (**159–161**), respectively.[136] All the modified dendrimers exhibit excellent solubility in common organic solvents except alcohol solution, fulfilling the requirements of fully solution-processable devices. As a result, fully solution-processed nondoped OLEDs with a device configuration of ITO/PEDOT-PSS (70 nm)/PVK (poly-vinylcarbazole, 20 nm)/EML (20–25 nm)/TPBi (40 nm)/Ca (10 nm)/Al (80 nm) were fabricated by spin-coating all organic materials. The maximum EQEs are 9.4% (**159**), 9.5% (**160**), and 8.2% (**161**), which are comparable to or even higher than those of the TPBi vacuum evaporated devices. Sun *et al.*[137] also designed self-host dendrimers **162** and **163** by connecting the emission core TCz-TRZ with the peripherally Cz-based host matrix through nonconjugated aliphatic chains. The prevalent concentration quenching effect of TADF materials can thus be effectively restrained by the encapsulation of the emissive core. Moreover, the device performances are found to be greatly dependent on the peripheral dendrons, suggesting the importance of the role in molecular modulation for performance improvement. Using the same self-host strategy, they also decorated the emitting core 4,4′,4″-(1,3,5-triazine-2,4,6-triyl) tris(*N*,*N*-diphenylaniline) (TTPA-TRZ) with Cz-based dendrons for high-performance solution-processed nondoped OLEDs (**164** and **165**).[138]

Choi *et al.*[139] also designed two dendrimers **166** and **167** by choosing the efficient nondoped green TADF material **142** as the emitting core. Using a methylene group as the linkage can effectively disrupt the conjugation between the peripheral Cz-based dendrons and the emitter core. Thus, the performances of the emitter core are independent of the dendrons. Their nondoped solution-processable OLEDs demonstrate acceptable performance with maximum EQEs of 9.5% for **166** and 8.1% for **167**.

In addition to the abovementioned TRZ-based dendrimers, the TRZ unit has also been applied to design novel polymers for solution-processed devices. Cheng *et al.*[140] reported a series of conjugated TADF polymers **168** by using conjugated acridine/carbazole and *t*Bu-substituted TRZ moieties as the backbones and pendant, respectively. The long alkyl branched chains significantly enhance the solubility of the target polymers in common solvents, which is very beneficial for the solution process. Meanwhile, the TADF core can be sparsely incorporated into the poly-3,6-carbazole backbone to realize molecular dispersion, and the distance between the adjacent TADF chromophores can flexibly be regulated through a subtly lengthened carbazole oligomer. Therefore, a high PLQY of 0.90 was realized with the 5% molar content of the TADF emission unit. They also modified **168** by replacing the *t*Bu group with phenyl units on the triazine parent (**169**).[141] Although introducing the Cz group is expected to isolate the TADF emission core and relieve the concentration quenching effect, all these constructed polymers still exhibit high concentration sensitivities, and this needs further in-depth study.

The conjugated acridine/carbazole backbones would lower the triplet excited state, which is detrimental to realizing the TADF characteristic. To realize high-performance TADF polymers, Wang *et al.*[142] proposed exploiting through-space CT polymers **170–173** containing a nonconjugated polystyrene backbone and spatially separated D and A units for solution-processed OLEDs. Such a molecular design strategy can not only avoid the large bathochromic shift of the TADF emission but also limit the electron cloud overlap of the FMOs, which is beneficial for reducing ΔE_{ST} and achieving TADF

Open Access Article. Published on 22 febbraio 2022. Downloaded on 08/05/2026 07:17:27.
This article is licensed under a Creative Commons Attribution-NonCommercial 3.0 Unported Licence.

characteristics. By further tuning the CT strengths, an emission color spanning from the deep blue (455 nm) to red (616 nm) region can be achieved. Meanwhile, by incorporating two kinds of D/A pairs into one polymer to create double through-space CT channels, blue and yellow emission can be simultaneously obtained, indicating that white electroluminescence can be realized from a single polymer. They also designed two through-space CT polymers **174** and **175** based on a nonconjugated poly(*cis*,*exo*-2,3-diarylnorbornene) backbone with D and A units fixed in edge-to-face/face-to-face alignment patterns.[143] Compared to its edge-to-face counterpart **174**, the **175** neat film with face-to-face aligned D/A units exhibits a much larger oscillator strength (*f*) and higher PLQY up to 0.81 owing to the enhanced spatial electron cloud overlaps. Therefore, the **175**-based solution-processed nondoped device realizes a maximum EQE of 18.8%, which is the best efficiency for blue TADF polymers thus far.

3.5. Boron-based units as acceptors

Due to the vacant p-orbital of boron atoms, triarylboron-based acceptors have been utilized to exploit emitters for optoelectronics. The molecular structures of boron-based TADF emitters are shown in Fig. 13, and the corresponding key parameters of the nondoped devices are summarized in Table 5. Lu *et al.*[144] reported two efficient blue TADF emitters **176** and **177** bearing triarylboron as the A group and *ortho*-positioned Cz and *t*Cz, respectively, as the D group. Such *ortho*-positioned D–A molecular structures favor the coexistence of through-bond and through-space CT processes, guaranteeing a high transition dipole moment and small ΔE_{ST}s. Moreover, both highly twisted

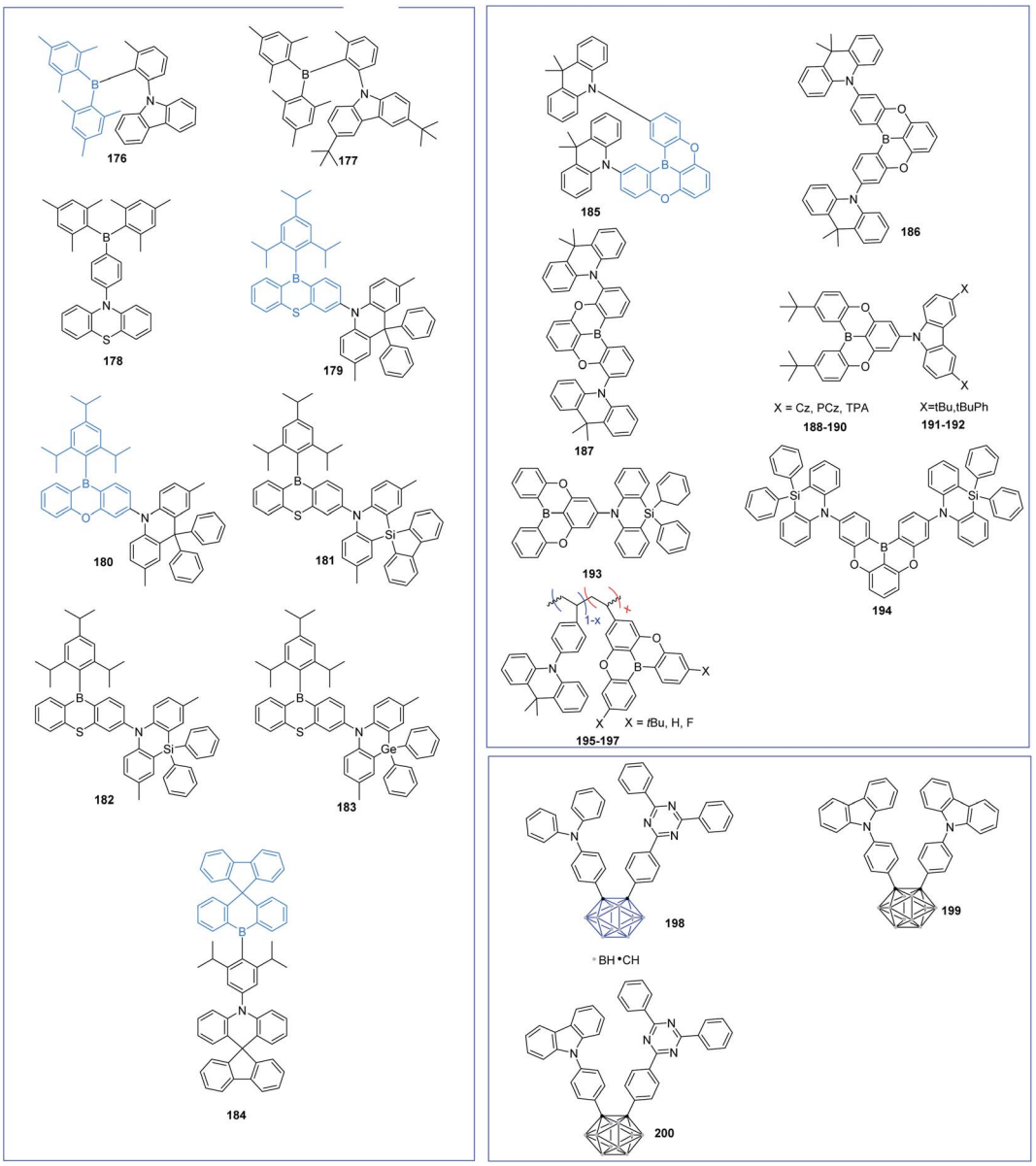

Fig. 13 Molecular structures of boron-based TADF emitters for nondoped OLEDs.

© 2022 The Author(s). Published by the Royal Society of Chemistry

Open Access Article. Published on 22 febbraio 2022. Downloaded on 08/05/2026 07:17:27.
This article is licensed under a Creative Commons Attribution-NonCommercial 3.0 Unported Licence.

Table 5 PL and EL properties of boron-based TADF emitters in nondoped films

	PL			EL						
						CE/PE/EQE [cd A^{-1}/lm W^{-1}/%]				
	PLQY	τ_p [ns]	τ_d [μs]	Peak [nm]	V_{on}[a] [V]	Maximum	@10^3 cd m^{-2}	Roll-off[b] [%]	CIE (x,y)	Ref.
176	0.61	52.0	15.0	463	4.4	11.6/7.6/8.0	3.8/1.5/2.6	67.5	(0.15, 0.17)	144
177	0.94	63.0	14.0	474	3.9	37.3/27.6/19.1	18.8/8.5/9.7	49.2	(0.15, 0.26)	
178	0.60	—	—	540	2.8	62.9/—/19.7	—/—/17.3	12.2	(0.37, 0.57)	145
179	0.99	7.5	1.7	487	3.4	49.9/41.4/22.8	—/—/19.0	16.7	(0.15, 0.36)	146
180	0.98	27.0	2.4	474	3.5	33.6/29.3/21.3	—/—/8.0	62.4	(0.14, 0.23)	
181	0.11	1.3	1.7	—	—	—	—	—	—	147
182	0.74	1.0	2.3	473	3.6	30.1/23.8/20.9	—/—/18.2	12.9	(014, 0.20)	
183	0.83	1.0	3.2	473	4.4	25.7/16.9/17.4	—/—/14.9	14.4	(014, 0.20)	
184	0.84	50.0	0.15	452	3.1	19.3/18.3/22.5	10.7/5.9/14.8	34.2	(0.16, 0.09)	148
185	0.73	98.8	4.4	—	—	—	—	—	—	149
186	0.94	62.3	1.8	516	2.7	44.3/47.1/14.1	39.5/27.6/12.7	9.9	(0.28, 0.54)	
187	0.70	145.7	8.1	—	—	—	—	—	—	
188	0.99	13.7	4.4	424	3.5	4.0/3.8/9.9	—	—	(0.17, 0.07)	150
189	0.93	18.5	4.7	448	3.0	4.6/4.1/6.1	—	—	(0.15, 0.08)	
190	0.90	15.7	5.4	492	2.6	15.0/15.7/6.0	—	—	(0.18, 0.40)	
191	0.41	16.4	1.49	416	3.7	2.2/2.0/8.2	—	—	(0.17, 0.06)	151
192	0.52	17.1	4.06	428	3.5	5.6/5.0/15.8	—	—	(0.16, 0.05)	
193	0.43	14.0	1.2	468	3.6	12.3/8.9/8.7	—/—/4.5	48.3	(0.15, 0.17)	33
194	0.73	13.0	1.6	464	3.2	40.9/36.0/23.1	—/—/13.0	43.7	(0.15, 0.20)	
195	0.37	—	—	451	3.8	5.8/5.1/3.8	—	—	(0.18, 0.17)	152
196	0.48	—	—	455	3.4	10.3/9.5/6.1	—	—	(0.18, 0.20)	
197	0.70	—	—	474	3.2	30.7/30.2/15.0	—	—	(0.16, 0.27)	
198	0.55	10.0	—	631	4.4	12.0/7.9/10.1	—	—	—	153
199	0.94	13.0	28.0	590	4.4	19.9/11.2/9.2	—	—	—	
200	0.97	15.0	27.0	586	6.3	16.7/7.6/11.0	—	—	—	

[a] Turn-on voltage at a luminance of 1 cd m^{-2}. [b] $EQE_{roll\text{-}off} = (EQE_{max} - EQE_{1000})/EQE_{max}$.

D/A moieties and steric alkyl substituents can efficiently inhibit aggregation-induced quenching. Meanwhile, compared with Cz-based emitter **176**, additional *t*Bu groups in **177** can not only improve the solubility, benefiting solution processing but also restrict the close intermolecular π–π packing. Therefore, solution-processed nondoped OLEDs using **176** and **177** as the EMLs achieve blue EL emission with peaks at 463 nm and 474 nm and maximum EQEs of 8.0% and 19.1%, respectively. By replacing the *t*BuCz unit in **177** with a butterfly shaped PTZ unit, Lu *et al.*[145] synthesized a novel boron-based TADF emitter **178**. Owing to the well-restricted intermolecular interactions, its amorphous neat film achieves a high PLQY of 0.65. The **178**-based nondoped device also obtains a high maximum EQE of 19.7%. It should be noted that there is a shoulder emission below 450 nm when **178** is doped in *m*CP with 5 wt%. The authors believe that this shoulder emission is due to the host material, but the EL emission of *m*CP cannot reach this position. We suspect that this emission arrives from the QA form of **178** caused by conformational isomerism of the PTZ group.

Yasuda *et al.*[146] developed a series of TADF materials with different bridging heteroatoms (sulfur for **179** and oxygen for **180**). Highly twisted D–A molecular structures with steric alkyl substituents benefit not only small ΔE_{ST}s but also well-restricted concentration quenching effects. Meanwhile, as shown in Fig. 14a, compared with oxygen-linked emitter **180**, incorporating a phenothiaborin (PTB) unit into **179** can significantly enhance the SOC effect, thereby accelerating the RISC and shortening the TADF emission lifetime to ~1 μs, which is among the shortest lifetimes ever reported for efficient TADF emitters and comparable to those of organometallic phosphorescent emitters. The **179**- and **180**-based nondoped devices attain considerably high EQEs of up to 22.8% and 21.3%, respectively. More importantly, owing to the short τ_d, the **179**-based device can still retain a high EQE of 19.0% at a high luminance of 1000 cd m^{-2}, much higher than that of **180** (an EQE of 8.0%) (shown in Fig. 14c). To further enhance the SOC effect, they also exploited a series of acridan analogues, phenazasiline and phenazagermine, with heavy elements in group 14 (silicon and germanium atoms). By using the same PTB unit as the weak A group, novel blue TADF emitters **181–183** were synthesized.[147] Incorporating larger silicon and germanium atoms can effectively enhance the structural flexibility of the D units, leading to conformational heterogeneity as well as dual fluorescence capability. Meanwhile, terminal bulky substituents can effectively suppress the ACQ, and thereby, high PLQY values of 0.74 and 0.83 are obtained for **182** and **183** neat films, respectively. Hence, **182**- and **183**-based nondoped devices demonstrate excellent EL performances, with maximum EQEs as high as 20.9% and 17.4%, respectively, and suppressed efficiency roll-off at practically high luminance.

Open Access Article. Published on 22 febbraio 2022. Downloaded on 08/05/2026 07:17:27.
This article is licensed under a Creative Commons Attribution-NonCommercial 3.0 Unported Licence.

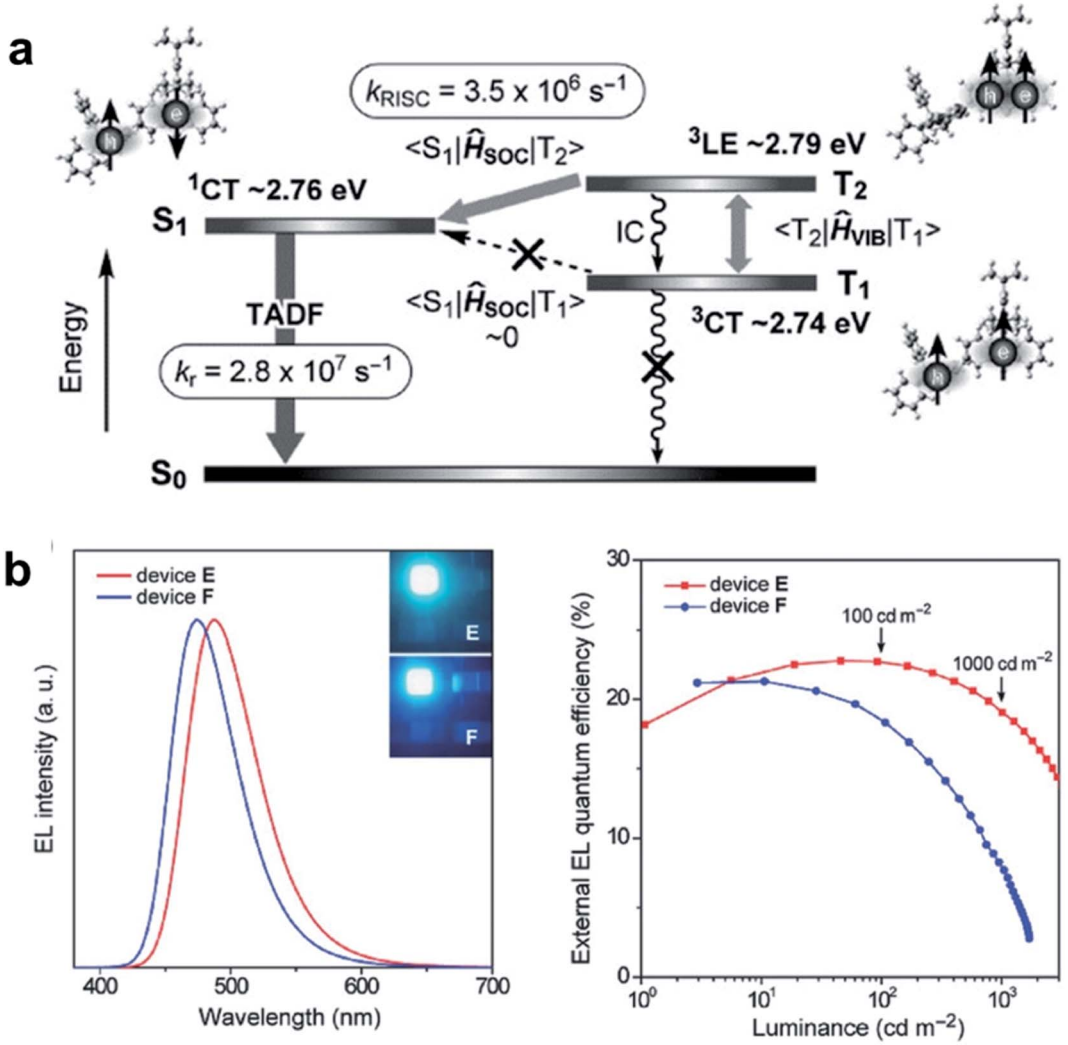

Fig. 14 (a) Schematic diagram for plausible RISC and TADF mechanisms involving SOC-induced spin conversion in **179**. (b) EL and EQE-L characteristics of the nondoped TADF-OLEDs (devices E and F based on **179** and **180**, respectively). Reproduced from ref. 146 with permission. Copyright 2018 Wiley-VCH.

Although TADF-based blue nondoped devices with maximum EQEs exceeding 20% have been achieved, it should be noted that their emissions are mostly in the sky-blue range with peaks at above 470 nm. In contrast, high-performance deep-blue TADF materials (<460 nm) for nondoped devices have been rarely reported. This is because developing them should not only consider the suppression of concentration quenching like with other color ones, but more importantly, it requires suitable D and A pairs that provide wide enough bandgaps. To achieve high-performance deep-blue nondoped OLEDs, Wang *et al.*[148] designed a deep-blue D–π–A-type TADF emitter **184** by combining SFAc and weak electron-withdrawing siprodipenozoborinine (sDBB) as the D and A moieties, respectively. Both the fluorene groups appended on D/A moieties and the bulky isopropyl group on the bridge unit can effectively suppress the intermolecular interactions of neighboring molecules. Therefore, the annoying concentration quenching can be well relieved. Moreover, bulky isopropyl groups can effectively restrict the molecular free rotations between the bridge and the A groups, benefiting a high PLQY and a narrow emission bandwidth. As a result, the corresponding nondoped device realizes a deep-blue EL emission with a maximum EQE of 22.5% and CIE_y < 0.1.

Boron-containing polycyclic aromatic hydrocarbons have emerged as very promising candidates for optoelectronic applications by virtue of their unique photophysical properties, good thermal stability, rigid planar structure, and easy structural modification. One typical framework is 5,9-dioxa-13*b*-boranaphtho[3,2,1-*de*]anthracene (DOBA) (1,3-diphenoxybenzene fused with a boron atom). Wang *et al.*[149] designed and synthesized three isomeric derivatives **185–187** by incorporating two DMAC units at different locations of two of the phenyl rings (wing phenyl groups) in the DOBA unit. The location and orientation of the DMAC unit significantly influence the physical properties of the three isomers. The *para*-substituted isomer **186** realizes a short τ_d of 1.8 μs and a higher PLQY value of 0.94 in the neat film state

© 2022 The Author(s). Published by the Royal Society of Chemistry

Open Access Article. Published on 22 febbraio 2022. Downloaded on 08/05/2026 07:17:27.
This article is licensed under a Creative Commons Attribution-NonCommercial 3.0 Unported Licence.

than the others. Therefore, the **186**-based nondoped device realizes a green EL emission with a peak at 516 nm, CIE coordinates of (0.28, 0.54), and a maximum EQE of 14.1%.

Choi *et al.*[150] also designed three DOBA-based TADF emitters **188–190** by tethering Cz-, PCz-, and DPA-substituted Cz derivatives (9′*H*-9,3′:6′,9″-tercarbazole, 9,9″-diphenyl-9*H*,9′*H*,9″*H*-3,3′:6′,3″-tercarbazole, and N^3,N^3,N^6,N^6-tetraphenyl-9*H*-carbazole-3,6-diamine) with the *t*Bu-substituted DOBA unit (2,12-di-*tert*-butyl-5,9-dioxa-13*b*-boranaphtho[3,2,1-*de*]anthracene). All emitters exhibit AIDF features and high PLQY values (>0.90). Consequently, solution-processed nondoped OLEDs fabricated using **188–190** as the EMLs exhibit maximum EQEs of 9.9%, 6.1%, and 6.0%. Moreover, the **188**- and **189**-based devices exhibit deep-blue EL emission with CIE coordinates of (0.17, 0.07) and (0.15, 0.08), respectively, which approach the NTSC blue standards. They also designed two ultradeep-blue AIDF emitters **191** and **192** by decorating prototype **188** with *t*Bu and *t*Bu phenyl units.[151] Owing to the large SOC effect arising from the closely located ^{1}CT state and ^{3}LE states, both emitters exhibit relatively fast k_{RISC} ($\sim 10^6$ s^{-1}), benefiting the upconversion process of the dark triplet excitons. The solution-processed nondoped devices exhibit ultradeep-blue emissions of 416–428 nm, high color purities with FWHMs of 42.2–44.4 nm, and CIE coordinates of ($x = 0.16$–0.17, $y = 0.05$–0.06). At the same time, the **192**-based nondoped device exhibits a superior performance with a maximum EQE of 15.8%, almost 2-fold higher than that of **191** (8.2%), due to its smaller ΔE_{ST}, larger SOC and faster k_{RISC}.

By using DOBA as the A moiety, Yasuda *et al.*[33] also designed two 10,10-diphenylphenazasiline (PASi)-based deep blue TADF emitters **193** and **194**. Both emitters exhibit efficient deep blue emission with high PLQYs of 0.81 and 0.98, respectively, along with rather short emission lifetimes of ~1 μs in their doped films. Therefore, the corresponding doped devices achieve extremely high maximum EQEs of 21.7% and 33.8% with CIE coordinates of (0.14, 0.10) and (0.14, 0.17), respectively, for **193** and **194**. Moreover, the **194**-based device displays well-relieved concentration quenching, which can be reasonably ascribed to the dual stable conformations of the PASi moiety. In particular, the **194**-based nondoped device can still maintain a high maximum EQE of 23.1%, which is among the highest values for nondoped deep blue TADF-OLEDs ever reported.

To exploit DOBA-based polymers for efficient solution-processed nondoped OLEDs, Wang *et al.*[152] developed a series of through-space CT blue polymers **195–197**. In these polymers, the DMAC and *t*Bu/H/F-decorated DOBA moieties are linked to the nonconjugated polystyrene backbone as pendants. Such molecular configurations can not only circumvent the influence of the main chain on material properties but also limit the electron cloud overlaps of the FMOs, which is beneficial for reducing the ΔE_{ST}s and achieving TADF characteristics. Solution-processed nondoped devices based on polymers **195**, **196**, and **197** with 10 mol% DOBA content exhibit blue emissions with peaks at 451, 455, and 474 nm and CIE coordinates of (0.18, 0.17), (0.18, 0.20) and (0.16, 0.27), respectively.

In addition to the abovementioned triarylboron derivatives, *o*-carborane (1,2-*closo*-dicarbadodecaborane ($C_2B_{10}H_{12}$)) is also known as an electron-deficient icosahedral boron cluster consisting of three-center two-electron bonds and possesses a highly polarizable σ-aromatic character. Based on this unique boron cluster, Yasuda *et al.*[153] developed a series of efficient AIDF emitters **198–200** for orange/red nondoped OLEDs. Due to their AIDF characteristics, all three emitters exhibit small ΔE_{ST}s and high PLQYs of up to 97% in solid-state neat films. In nondoped devices, superior performances are realized with maximum EQEs of 10.1%, 9.2%, and 11.0% for **198**, **199**, and **200**, respectively.

4. Conclusion and outlook

Since the pioneering work of Prof. Adachi *et al.*, TADF materials have demonstrated explosive development and gradually expanded from OLEDs to the fields of photocatalysis, biomedical applications, electrochemical cells, *etc.* As a special category, TADF materials for nondoped OLEDs are a hot research area due to the advantages of high efficiency, structural or process simplicity, and avoidance of potential phase-separation problems faced in host–guest systems. In this review, we mainly discussed TADF emitters for nondoped devices, including the mechanism, exciton leaking channels, molecular design strategies, and molecular structures based on functional A groups. Using materials with AIE/AIDF features or intermolecular hydrogen bonding can effectively suppress nonradiative transitions, while the most important issue for high-performance nondoped OLEDs is to suppress exciton annihilation, especially related to triplet excitons. Based on this, the reported molecular design strategies can be broadly divided into the following two categories: the first is to increase the core distances of the adjacent luminescent materials, such as by introducing large steric hindrance groups or host matrixes with wide bandgaps, applying molecular conformational isomerization, and properly utilizing weak intermolecular interactions (*e.g.*, hydrogen bonding); the other is to design molecules with D–spacer–A molecular skeletons to induce intermolecular CT rather than intermolecular exciton annihilation. By utilizing these molecular design strategies, many efficient nondoped devices with neglectable efficiency roll-off at high luminance have been successfully developed in the past decade. However, their development is still facing some challenges, which need further in-depth investigations. Firstly, compared with the blue and green counterparts that have achieved maximum EQEs of over 20%, the development pace of the red counterparts seriously lags behind due to the inherent narrow bandgaps causing severe exciton losses. Secondly, the operational stability of OLEDs is also an important indicator in determining commercial mass production, but it has seldom been considered in nondoped OLEDs. The few reports of TADF-based nondoped OLEDs that mentioned operational measurements all showed very short operational lifetimes, lagging far behind the development of doped OLEDs. The less satisfactory operational stability of current reported non-doped devices can be mainly attributed to the following two aspects: (i) the employed emitters generally have less stable chemical structures that contain weak bonds; (ii) k_{RISC}s are not high enough, resulting in

Open Access Article. Published on 22 febbraio 2022. Downloaded on 08/05/2026 07:17:27.
This article is licensed under a Creative Commons Attribution-NonCommercial 3.0 Unported Licence.

accumulation and quenching of long-lived triplet excitons particularly at high voltages in the EML. Therefore, exploiting TADF emitters with stable chemical structures and short τ_ds to dilute exciton concentrations should be the main pursuits to improve the operational lifetimes of TADF-based nondoped OLEDs. In addition, MR-TADF emitters have recently attracted tremendous attention due to their excellent color purities and device efficiencies. However, due to their typical rigid and planar molecular structures, precise modulation of doping weight is still necessary to achieve these superior device performances. How to effectively suppress its concentration sensitivity without affecting the light-emission wavelengths and color purity is still unknown and needs further in-depth study. Despite the current challenges, exploiting novel TADF emitters for high-performance nondoped OLEDs remains an important research direction at the current stage.

Author contributions

X. H. Zhang and K. Wang conceived the idea of the review and supervised the work. Y. Z. Shi, J. Yu and X. M. Ou designed the structure of the article. Y. Z. Shi and H. Wu conducted the bibliographic research. H. Wu contributed to an early draft, and Y. Z. Shi and K. Wang wrote the manuscript. All the authors participated in the revision of the manuscript.

Conflicts of interest

The authors declare no conflicts of interest.

Acknowledgements

This work was supported by the National Key Research & Development Program of China (Grant No. 2020YFA0714601, 2020YFA0714604), the National Natural Science Foundation of China (Grant No. 52130304, 51821002, 52003185, 52003186), the China Postdoctoral Science Foundation (Grant No. 2019M661924), Suzhou Key Laboratory of Functional Nano & Soft Materials, Collaborative Innovation Center of Suzhou Nano Science & Technology, the 111 Project, and Joint International Research Laboratory of Carbon-Based Functional Materials and Devices.

References

1 C. W. Tang and S. A. VanSlyke, *Appl. Phys. Lett.*, 1987, **51**, 913–915.
2 M. A. Baldo, D. F. O'Brien, Y. You, A. Shoustikov, S. Sibley, M. E. Thompson and S. R. Forrest, *Nature*, 1998, **395**, 151–154.
3 H. Uoyama, K. Goushi, K. Shizu, H. Nomura and C. Adachi, *Nature*, 2012, **492**, 234–238.
4 K. Goushi, K. Yoshida, K. Sato and C. Adachi, *Nat. Photonics*, 2012, **6**, 253–258.
5 Q. Zhang, B. Li, S. Huang, H. Nomura, H. Tanaka and C. Adachi, *Nat. Photonics*, 2014, **8**, 326–332.
6 C. Y. Chan, M. Tanaka, Y. T. Lee, Y. W. Wong, H. Nakanotani, T. Hatakeyama and C. Adachi, *Nat. Photonics*, 2021, **15**, 203–207.
7 X. Y. Cai and S. J. Su, *Adv. Funct. Mater.*, 2018, **28**, 1802558.
8 M. Y. Wong and E. Zysman-Colman, *Adv. Mater.*, 2017, **29**, 1605444.
9 Q. Wei, N. Fei, A. Islam, T. Lei, L. Hong, R. Peng, X. Fan, L. Chen, P. Gao and Z. Ge, *Adv. Opt. Mater.*, 2018, **6**, 1800512.
10 Y. Zou, S. L. Gong, G. H. Xie and C. L. Yang, *Adv. Opt. Mater.*, 2018, **6**, 1800568.
11 M. Sarma and K. T. Wong, *ACS Appl. Mater. Interfaces*, 2018, **10**, 19279–19304.
12 P. Xiao, J. H. Huang, Y. C. Yu, J. Yuan, D. X. Luo, B. Q. Liu and D. Liang, *Appl. Sci.*, 2018, **8**, 1449.
13 Q. Wang, Q. S. Tian, Y. L. Zhang, X. Tang and L. S. Liao, *J. Mater. Chem. C*, 2019, **7**, 11329–11360.
14 M. Zhang, C. J. Zheng, H. Lin and S. L. Tao, *Mater. Horiz.*, 2020, **8**, 401–425.
15 X. K. Liu, Z. Chen, C. J. Zheng, C. L. Liu, C. S. Lee, F. Li, X. M. Ou and X. H. Zhang, *Adv. Mater.*, 2015, **27**, 2378–2383.
16 W. Liu, J. X. Chen, C. J. Zheng, K. Wang, D. Y. Chen, F. Li, Y. P. Dong, C. S. Lee, X. M. Ou and X. H. Zhang, *Adv. Funct. Mater.*, 2016, **26**, 2002–2008.
17 M. Zhang, W. Liu, C. J. Zheng, K. Wang, Y. Z. Shi, X. Li, H. Lin, S. L. Tao and X. H. Zhang, *Adv. Sci.*, 2019, **6**, 1801938.
18 J. M. Ha, S. H. Hur, A. Pathak, J.-E. Jeong and H. Y. Woo, *NPG Asia Mater.*, 2021, **13**, 53.
19 M. Hirai, N. Tanaka, M. Sakai and S. Yamaguchi, *Chem. Rev.*, 2019, **119**, 8291–8331.
20 S. Madayanad Suresh, D. Hall, D. Beljonne, Y. Olivier and E. Zysman-Colman, *Adv. Funct. Mater.*, 2020, **30**, 1908677.
21 S. Gan, S. Hu, X. L. Li, J. Zeng, D. Zhang, T. Huang, W. Luo, Z. Zhao, L. Duan, S. J. Su and B. Z. Tang, *ACS Appl. Mater. Interfaces*, 2018, **10**, 17327–17334.
22 J. Xu, X. Zhu, J. Guo, J. Fan, J. Zeng, S. Chen, Z. Zhao and B. Z. Tang, *ACS Mater. Lett.*, 2019, **1**, 613–619.
23 A. Kretzschmar, C. Patze, S. T. Schwaebel and U. H. F. Bunz, *J. Org. Chem.*, 2015, **80**, 9126–9131.
24 T. Huang, X. Song, M. Cai, D. Zhang and L. Duan, *Mater. Today Energy*, 2021, **21**, 100705.
25 M. K. Etherington, J. Gibson, H. F. Higginbotham, T. J. Penfold and A. P. Monkman, *Nat. Commun.*, 2016, **7**, 13680–13686.
26 M. K. Etherington, F. Franchello, J. Gibson, T. Northey, J. Santos, J. S. Ward, H. F. Higginbotham, P. Data, A. Kurowska, P. L. Dos Santos, D. R. Graves, A. S. Batsanov, F. B. Dias, M. R. Bryce, T. J. Penfold and A. P. Monkman, *Nat. Commun.*, 2017, **8**, 14987–14997.
27 J. X. Chen, Y. F. Xiao, K. Wang, D. Sun, X. C. Fan, X. Zhang, M. Zhang, Y. Z. Shi, J. Yu, F. X. Geng, C. S. Lee and X. H. Zhang, *Angew. Chem., Int. Ed.*, 2021, **60**, 2478–2484.
28 X. C. Fan, K. Wang, Y. Z. Shi, J. X. Chen, F. Huang, H. Wang, Y. N. Hu, Y. Tsuchiya, X. M. Ou, J. Yu, C. Adachi and X. H. Zhang, *Adv. Opt. Mater.*, 2022, **10**, 2101789.

© 2022 The Author(s). Published by the Royal Society of Chemistry

Open Access Article. Published on 22 febbraio 2022. Downloaded on 08/05/2026 07:17:27.
This article is licensed under a Creative Commons Attribution-NonCommercial 3.0 Unported Licence.

29 D. R. Lee, B. S. Kim, C. W. Lee, Y. Im, K. S. Yook, S. H. Hwang and J. Y. Lee, *ACS Appl. Mater. Interfaces*, 2015, **7**, 9625–9629.
30 D. Karthik, Y. H. Jung, H. Lee, S. Hwang, B. M. Seo, J. Y. Kim, C. W. Han and J. H. Kwon, *Adv. Mater.*, 2021, **33**, 2007724.
31 W. Zeng, H. Y. Lai, W. K. Lee, M. Jiao, Y. J. Shiu, C. Zhong, S. Gong, T. Zhou, G. Xie, M. Sarma, K. T. Wong, C. C. Wu and C. Yang, *Adv. Mater.*, 2018, **30**, 1704961.
32 C. Zhang, D. Zhang, Z. Bin, Z. Liu, Y. Zhang, H. Lee, J. H. Kwon and L. Duan, *Adv. Mater.*, 2021, 2103102.
33 I. S. Park, H. Min, J. U. Kim and T. Yasuda, *Adv. Opt. Mater.*, 2021, **9**, 2101282.
34 M. Kim and J. Y. Lee, *Adv. Funct. Mater.*, 2014, **24**, 4164–4169.
35 Y. L. Zhang, Q. Ran, Q. Wang, Y. Liu, C. Hanisch, S. Reineke, J. Fan and L. S. Liao, *Adv. Mater.*, 2019, **31**, 1902368.
36 C. C. Peng, S. Y. Yang, H. C. Li, G. H. Xie, L. S. Cui, S. N. Zou, C. Poriel, Z. Q. Jiang and L. S. Liao, *Adv. Mater.*, 2020, **32**, 2003885.
37 H. Xu, Z. Li, D. Yang, C. Han, B. Zhao, H. Wang, P. Ma, P. Chang and D. Ma, *Angew. Chem., Int. Ed.*, 2021, **60**, 14846–14851.
38 M. Ma, J. Li, D. Liu, Y. Mei and R. Dong, *ACS Appl. Mater. Interfaces*, 2021, **13**, 44615–44627.
39 J. X. Chen, K. Wang, Y. F. Xiao, C. Cao, J. H. Tan, H. Wang, X. C. Fan, J. Yu, F. X. Geng, X. H. Zhang and C. S. Lee, *Adv. Funct. Mater.*, 2021, **31**, 2101647.
40 M. Godumala, S. Choi, M. J. Cho and D. H. Choi, *J. Mater. Chem. C*, 2019, **7**, 2172–2198.
41 D. Mobius, *Adv. Mater.*, 1995, **7**, 437–444.
42 F. Wurthner, *Angew. Chem., Int. Ed.*, 2020, **59**, 14192–14196.
43 J. Luo, Z. Xie, J. W. Lam, L. Cheng, H. Chen, C. Qiu, H. S. Kwok, X. Zhan, Y. Liu, D. Zhu and B. Z. Tang, *Chem. Commun.*, 2001, **18**, 1740–1741.
44 J. Huang, H. Nie, J. Zeng, Z. Zhuang, S. Gan, Y. Cai, J. Guo, S. J. Su, Z. Zhao and B. Z. Tang, *Angew. Chem., Int. Ed.*, 2017, **56**, 12971–12976.
45 K. Y. Sun, D. Liu, W. W. Tian, F. Gu, W. X. Wang, Z. S. Cai, W. Jiang and Y. M. Sun, *J. Mater. Chem. C*, 2020, **8**, 11850–11859.
46 J. Lee, N. Aizawa, M. Numata, C. Adachi and T. Yasuda, *Adv. Mater.*, 2017, **29**, 1604856.
47 X. Ban, F. Chen, Y. Liu, J. Pan, A. Zhu, W. Jiang and Y. Sun, *Chem. Sci.*, 2019, **10**, 3054–3064.
48 S. Wang, H. Zhang, B. Zhang, Z. Xie and W. Y. Wong, *Mater. Sci. Eng., A*, 2020, **140**, 100547.
49 Y. Z. Shi, K. Wang, S. L. Zhang, X. C. Fan, Y. Tsuchiya, Y. T. Lee, G. L. Dai, J. X. Chen, C. J. Zheng, S. Y. Xiong, X. M. Ou, J. Yu, J. S. Jie, C. S. Lee, C. Adachi and X. H. Zhang, *Angew. Chem., Int. Ed.*, 2021, **60**, 25878–25883.
50 Y. Shi, K. Wang, Y. Tsuchiya, W. Liu, T. Komino, X. Fan, D. Sun, G. Dai, J. Chen, M. Zhang, C. Zheng, S. Xiong, X. Ou, J. Yu, J. Jie, C.-S. Lee, C. Adachi and X. Zhang, *Mater. Horiz.*, 2020, **7**, 2734–2740.
51 Y. Z. Shi, K. Wang, X. Li, G. L. Dai, W. Liu, K. Ke, M. Zhang, S. L. Tao, C. J. Zheng, X. M. Ou and X. H. Zhang, *Angew. Chem., Int. Ed.*, 2018, **57**, 9480–9484.
52 D. Gudeika, O. Bezvikonnyi, D. Volyniuk and J. V. Grazulevicius, *Dyes Pigm.*, 2020, **172**, 107789.
53 X. Zheng, R. Huang, C. Zhong, G. Xie, W. Ning, M. Huang, F. Ni, F. B. Dias and C. Yang, *Adv. Sci.*, 2020, **7**, 1902087.
54 Z. Cheng, Z. Li, Y. Xu, J. Liang, C. Lin, J. Wei and Y. Wang, *ACS Appl. Mater. Interfaces*, 2019, **11**, 28096–28105.
55 Z. Cheng, J. Liang, Z. Li, T. Yang, C. Lin, X. Mu and Y. Wang, *J. Mater. Chem. C*, 2019, **7**, 14255–14263.
56 D. Zhang, M. Cai, Y. Zhang, D. Zhang and L. Duan, *Mater. Horiz.*, 2016, **3**, 145–151.
57 C. Y. Chan, M. Tanaka, H. Nakanotani and C. Adachi, *Nat. Commun.*, 2018, **9**, 5036.
58 X. Ban, Y. Liu, J. Pan, F. Chen, A. Zhu, W. Jiang, Y. Sun and Y. Dong, *ACS Appl. Mater. Interfaces*, 2019, **12**, 1190–1200.
59 S. J. Zou, F. M. Xie, M. Xie, Y. Q. Li, T. Cheng, X. H. Zhang, C. S. Lee and J. X. Tang, *Adv. Sci.*, 2019, **7**, 1902508.
60 D. Liu, M. Zhang, H. Chen, D. Ma, W. Tian, K. Sun, W. Jiang and Y. Sun, *J. Mater. Chem. C*, 2020, **9**, 1221–1227.
61 H. Noda, H. Nakanotani and C. Adachi, *Sci. Adv.*, 2018, **4**, 6910.
62 Y. J. Cho, S. K. Jeon and J. Y. Lee, *Adv. Opt. Mater.*, 2016, **4**, 688–693.
63 X. Ban, A. Zhu, T. Zhang, Z. Tong, W. Jiang and Y. Sun, *ACS Appl. Mater. Interfaces*, 2017, **9**, 21900–21908.
64 D. Liu, W. Tian, Y. Feng, X. Zhang, X. Ban, W. Jiang and Y. Sun, *ACS Appl. Mater. Interfaces*, 2019, **11**, 16737–16748.
65 J. Y. Wei, D. Liu, W. W. Tian, W. Jiang, Y. M. Sun, Z. Zhao and B. Z. Tang, *Chem. Sci.*, 2020, **11**, 7194–7203.
66 H. J. Kim, S. K. Kim, M. Godumala, J. W. Yoon, C. Y. Kim, J. E. Jeong, H. Y. Woo, J. H. Kwon, M. J. Cho and D. H. Choi, *Chem. Commun.*, 2019, **55**, 9475–9478.
67 C. Wu, Z. Wu, B. Wang, X. Li, N. Zhao, J. Hu, D. Ma and Q. Wang, *ACS Appl. Mater. Interfaces*, 2017, **9**, 32946–32956.
68 M. K. Etherington, N. A. Kukhta, H. F. Higginbotham, A. Danos, A. N. Bismillah, D. R. Graves, P. R. McGonigal, N. Haase, A. Morherr, A. S. Batsanov, C. Pflumm, V. Bhalla, M. R. Bryce and A. P. Monkman, *J. Phys. Chem. C*, 2019, **123**, 11109–11117.
69 K. Sun, Y. Sun, W. Tian, D. Liu, Y. Feng, Y. Sun and W. Jiang, *J. Mater. Chem. C*, 2018, **6**, 43–49.
70 Z. G. Wu, H. B. Han, Z. P. Yan, X. F. Luo, Y. Wang, Y. X. Zheng, J. L. Zuo and Y. Pan, *Adv. Mater.*, 2019, **31**, 1900524.
71 Z. G. Wu, Z. P. Yan, X. F. Luo, L. Yuan, W. Q. Liang, Y. Wang, Y. X. Zheng, J. L. Zuo and Y. Pan, *J. Mater. Chem. C*, 2019, **7**, 7045–7052.
72 Q. Zhang, D. Tsang, H. Kuwabara, Y. Hatae, B. Li, T. Takahashi, S. Y. Lee, T. Yasuda and C. Adachi, *Adv. Mater.*, 2015, **27**, 2096–2100.
73 Y. Li, G. Xie, S. Gong, K. Wu and C. Yang, *Chem. Sci.*, 2016, **7**, 5441–5447.
74 Y. Yang, S. Wang, Y. Zhu, Y. Wang, H. Zhan and Y. Cheng, *Adv. Funct. Mater.*, 2018, **28**, 1706916.

Open Access Article. Published on 22 febbraio 2022. Downloaded on 08/05/2026 07:17:27.
This article is licensed under a Creative Commons Attribution-NonCommercial 3.0 Unported Licence.

75 B. Huang, X. Ban, K. Sun, Z. Ma, Y. Mei, W. Jiang, B. Lin and Y. Sun, *Dyes Pigm.*, 2016, **133**, 380–386.
76 K. Matsuoka, K. Albrecht, K. Yamamoto and K. Fujita, *Sci. Rep.*, 2017, **7**, 41780–41788.
77 K. Matsuoka, K. Albrecht, A. Nakayama, K. Yamamoto and K. Fujita, *ACS Appl. Mater. Interfaces*, 2018, **10**, 33343–33352.
78 Y. Chen, S. Wang, X. Wu, Y. Xu, H. Li, Y. Liu, H. Tong and L. Wang, *J. Mater. Chem. C*, 2018, **6**, 12503–12508.
79 Y. Liu, X. Wu, Y. Chen, L. Chen, H. Li, S. Wang, H. Tian, H. Tong and L. Wang, *J. Mater. Chem. C*, 2019, **7**, 9719–9725.
80 L. Wang, X. Cai, B. Li, M. Li, Z. Wang, L. Gan, Z. Qiao, W. Xie, Q. Liang, N. Zheng, K. Liu and S. J. Su, *ACS Appl. Mater. Interfaces*, 2019, **11**, 45999–46007.
81 J. Guo, X. L. Li, H. Nie, W. Luo, S. Gan, S. Hu, R. Hu, A. Qin, Z. Zhao, S. J. Su and B. Z. Tang, *Adv. Funct. Mater.*, 2017, **27**, 1606458.
82 J. Guo, X. L. Li, H. Nie, W. Luo, R. Hu, A. Qin, Z. Zhao, S. J. Su and B. Z. Tang, *Chem. Mater.*, 2017, **29**, 3623–3631.
83 X. Chen, Z. Yang, Z. Xie, J. Zhao, Z. Yang, Y. Zhang, M. P. Aldred and Z. Chi, *Mater. Chem. Front.*, 2018, **2**, 1017–1023.
84 Y. Y. Jing, X. D. Tao, M. X. Yang, X. L. Chen and C. Z. Lu, *Chem. Eng. J.*, 2021, **413**, 127418.
85 J. Guo, J. Fan, L. Lin, J. Zeng, H. Liu, C. K. Wang, Z. Zhao and B. Z. Tang, *Adv. Sci.*, 2019, **6**, 1801629.
86 F. Ma, G. Zhao, Y. Zheng, F. He, K. Hasrat and Z. Qi, *ACS Appl. Mater. Interfaces*, 2019, **12**, 1179–1189.
87 H. Liu, J. Zeng, J. Guo, H. Nie, Z. Zhao and B. Z. Tang, *Angew. Chem., Int. Ed.*, 2018, **57**, 9290–9294.
88 H. Liu, H. Liu, J. Fan, J. Guo, J. Zeng, F. Qiu, Z. Zhao and B. Z. Tang, *Adv. Opt. Mater.*, 2020, **8**, 2001027.
89 F. Ma, X. Zhao, H. Ji, D. Zhang, K. Hasrat and Z. Qi, *J. Mater. Chem. C*, 2020, **8**, 12272–12283.
90 Z. Qiu, W. Xie, Z. Yang, J. H. Tan, Z. Yuan, L. Xing, S. Ji, W. C. Chen, Y. Huo and S. J. Su, *Chem. Eng. J.*, 2021, **415**, 128949.
91 N. Aizawa, C. J. Tsou, I. S. Park and T. Yasuda, *Polym. J.*, 2016, **49**, 197–202.
92 J. Chen, J. Zeng, X. Zhu, J. Guo, Z. Zhao and B. Z. Tang, *CCS Chem.*, 2021, **3**, 230–240.
93 L. Meng, H. Wang, X. Wei, J. Liu, Y. Chen, X. Kong, X. Lv, P. Wang and Y. Wang, *ACS Appl. Mater. Interfaces*, 2016, **8**, 20955–20961.
94 S. Xiang, R. Guo, Z. Huang, X. Lv, S. Sun, H. Chen, Q. Zhang and L. Wang, *Dyes Pigm.*, 2019, **170**, 107636.
95 J. Lee, N. Aizawa and T. Yasuda, *Chem. Mater.*, 2017, **29**, 8012–8020.
96 L. Wu, K. Wang, C. Wang, X. C. Fan, Y. Z. Shi, X. Zhang, S. L. Zhang, J. Ye, C. J. Zheng, Y. Q. Li, J. Yu, X. M. Ou and X. H. Zhang, *Chem. Sci.*, 2021, **12**, 1495–1502.
97 Z. Huang, Z. Bin, R. Su, F. Yang, J. Lan and J. You, *Angew. Chem., Int. Ed.*, 2020, **59**, 9992–9996.
98 M. Shibano, H. Ochiai, K. Suzuki, H. Kamitakahara, H. Kaji and T. Takano, *Macromolecules*, 2020, **53**, 2864–2873.
99 J. Li, R. Zhang, Z. Wang, B. Zhao, J. Xie, F. Zhang, H. Wang and K. Guo, *Adv. Opt. Mater.*, 2018, **6**, 1701256.
100 I. H. Lee, W. Song and J. Y. Lee, *Org. Electron.*, 2016, **29**, 22–26.
101 H. Tanaka, K. Shizu, H. Nakanotani and C. Adachi, *J. Phys. Chem. C*, 2014, **118**, 15985–15994.
102 J. Luo, S. Gong, Y. Gu, T. Chen, Y. Li, C. Zhong, G. Xie and C. Yang, *J. Mater. Chem. C*, 2016, **4**, 2442–2446.
103 X. Ban, W. Jiang, K. Sun, B. Lin and Y. Sun, *ACS Appl. Mater. Interfaces*, 2017, **9**, 7339–7346.
104 S. Xiang, z. huang, S. Sun, X. Lv, L. Fan, S. Ye, H. Chen, R. Guo and L. Wang, *J. Mater. Chem. C*, 2018, **6**, 11436–11443.
105 R. S. Nobuyasu, Z. Ren, G. C. Griffiths, A. S. Batsanov, P. Data, S. Yan, A. P. Monkman, M. R. Bryce and F. B. Dias, *Adv. Opt. Mater.*, 2016, **4**, 597–607.
106 Y. F. Li, T. H. Chen, M. L. Huang, Y. Gu, S. L. Gong, G. H. Xie and C. L. Yang, *J. Mater. Chem. C*, 2017, **5**, 3480–3487.
107 Z. Yang, Z. Mao, C. Xu, X. Chen, J. Zhao, Z. Yang, Y. Zhang, W. Wu, S. Jiao, Y. Liu, M. P. Aldred and Z. Chi, *Chem. Sci.*, 2019, **10**, 8129–8134.
108 C. S. Li, A. K. Harrison, Y. C. Liu, Z. N. Zhao, C. Zeng, F. B. Dias, Z. J. Ren, S. K. Yan and M. R. Bryce, *Angew. Chem., Int. Ed.*, 2021, DOI: 10.1002/anie.202115140.
109 R. Guo, P. Leng, Q. Zhang, Y. Wang, X. Lv, S. Sun, S. Ye, Y. Duan and L. Wang, *Dyes Pigm.*, 2020, **184**, 108781.
110 S. Reineke, F. Lindner, G. Schwartz, N. Seidler, K. Walzer, B. Lüssem and K. Leo, *Nature*, 2009, **459**, 234–239.
111 Y. Z. Shi, K. Wang, X. C. Fan, J. X. Chen, X. M. Ou, J. Yu, J. S. Jie, C. S. Lee and X. H. Zhang, *Adv. Opt. Mater.*, 2021, **9**, 2100461.
112 X. Li, S. Shen, C. Zhang, M. Liu, J. Lu and L. Zhu, *Sci. China: Chem.*, 2021, **64**, 534–546.
113 P. L. dos Santos, M. K. Etherington and A. P. Monkman, *J. Mater. Chem. C*, 2018, **6**, 4842–4853.
114 K. Wang, Y. Z. Shi, C. J. Zheng, W. Liu, K. Liang, X. Li, M. Zhang, H. Lin, S. L. Tao, C. S. Lee, X. M. Ou and X. H. Zhang, *ACS Appl. Mater. Interfaces*, 2018, **10**, 31515–31525.
115 K. Wang, C. J. Zheng, W. Liu, K. Liang, Y. Z. Shi, S. L. Tao, C. S. Lee, X. M. Ou and X. H. Zhang, *Adv. Mater.*, 2017, **29**, 1701476.
116 L. Zhang, Y. F. Wang, M. Li, Q. Y. Gao and C. F. Chen, *Chin. Chem. Lett.*, 2020, **32**, 740–744.
117 L. Yu, Z. Wu, G. Xie, W. Zeng, D. Ma and C. Yang, *Chem. Sci.*, 2018, **9**, 1385–1391.
118 L. Yu, Z. Wu, G. Xie, C. Zhong, Z. Zhu, D. Ma and C. Yang, *Chem. Commun.*, 2018, **54**, 1379–1382.
119 Y. Tao, D. Zhang, X. Cao, Q. Wu, M. Zhang, N. Sun and X. Zhang, *J. Mater. Chem. C*, 2017, **6**, 3675–3682.
120 X. Zhang, M. W. Cooper, Y. Zhang, C. Fuentes-Hernandez, S. Barlow, S. R. Marder and B. Kippelen, *ACS Appl. Mater. Interfaces*, 2019, **11**, 12693–12698.
121 S. Wang, X. Yan, Z. Cheng, H. Zhang, Y. Liu and Y. Wang, *Angew. Chem., Int. Ed.*, 2015, **54**, 13068–13072.
122 H. Xu, B. Zhao, H. Wang, C. Han, P. Ma, Z. Li and P. Chang, *Angew. Chem., Int. Ed.*, 2020, **59**, 19042–19047.

© 2022 The Author(s). Published by the Royal Society of Chemistry

Open Access Article. Published on 22 febbraio 2022. Downloaded on 08/05/2026 07:17:27.
This article is licensed under a Creative Commons Attribution-NonCommercial 3.0 Unported Licence.

123 H. Wang, B. Zhao, P. Ma, Z. Li, X. Wang, C. Zhao, X. Fan, L. Tao, C. Duan, J. Zhang, C. Han, G. Chen and H. Xu, *J. Mater. Chem. C*, 2019, **7**, 7525–7530.
124 J. X. Chen, W. W. Tao, W. C. Chen, Y. F. Xiao, K. Wang, C. Cao, J. Yu, S. Li, F. X. Geng, C. Adachi, C. S. Lee and X. H. Zhang, *Angew. Chem., Int. Ed.*, 2019, **58**, 14660–14665.
125 Y. Liu, Y. Chen, H. Li, S. Wang, X. Wu, H. Tong and L. Wang, *ACS Appl. Mater. Interfaces*, 2020, **12**, 30652–30658.
126 W. L. Tsai, M. H. Huang, W. K. Lee, Y. J. Hsu, K. C. Pan, Y. H. Huang, H. C. Ting, M. Sarma, Y. Y. Ho, H. C. Hu, C. C. Chen, M. T. Lee, K. T. Wong and C. C. Wu, *Chem. Commun.*, 2015, **51**, 13662–13665.
127 Y. Wada, K. Shizu, S. Kubo, T. Fukushima, T. Miwa, H. Tanaka, C. Adachi and H. Kaji, *Appl. Phys. Express*, 2016, **9**, 032102.
128 S. Jeong, Y. Lee, J. K. Kim, D. J. Jang and J. I. Hong, *J. Mater. Chem. C*, 2018, **6**, 9049–9054.
129 X. Cai, Z. Qiao, M. Li, X. Wu, Y. He, X. Jiang, Y. Cao and S. J. Su, *Angew. Chem., Int. Ed.*, 2019, **58**, 13522–13531.
130 W. Li, B. Li, X. Cai, L. Gan, Z. Xu, W. Li, K. Liu, D. Chen and S. J. Su, *Angew. Chem., Int. Ed.*, 2019, **58**, 11301–11305.
131 Q. Zhang, S. Sun, W. Liu, P. Leng, X. Lv, Y. Wang, H. Chen, S. Ye, S. Zhuang and L. Wang, *J. Mater. Chem. C*, 2019, **7**, 9487–9495.
132 X. Wang, S. Wang, J. Lv, S. Shao, L. Wang, X. Jing and F. Wang, *Chem. Sci.*, 2019, **10**, 2915–2923.
133 P. Zhang, J. Zeng, J. Guo, S. Zhen, B. Xiao, Z. Wang, Z. Zhao and B. Z. Tang, *Front. Chem.*, 2019, **7**, 199.
134 H. Y. Chih, Y. W. Chen, Y. C. Hsieh, W. C. Li, C. W. Liao, C. H. Lin, T. Y. Chiu, W. W. Tsai, C. W. Lu and C. H. Chang, *Chem.–Eur. J.*, 2019, **25**, 16699–16711.
135 K. Albrecht, K. Matsuoka, K. Fujita and K. Yamamoto, *Angew. Chem., Int. Ed.*, 2015, **54**, 5677–5682.
136 K. Albrecht, K. Matsuoka, D. Yokoyama, Y. Sakai, A. Nakayama, K. Fujita and K. Yamamoto, *Chem. Commun.*, 2017, **53**, 2439–2442.
137 X. Ban, W. Jiang, T. Lu, X. Jing, Q. Tang, S. Huang, K. Sun, B. Huang, B. Lin and Y. Sun, *J. Mater. Chem. C*, 2016, **4**, 8810–8816.
138 K. Sun, Y. Sun, T. Huang, J. Luo, W. Jiang and Y. Sun, *Org. Electron.*, 2017, **42**, 123–130.
139 M. Godumala, S. Choi, H. J. Kim, C. Lee, S. Park, J. S. Moon, K. Si Woo, J. H. Kwon, M. J. Cho and D. H. Choi, *J. Mater. Chem. C*, 2018, **6**, 1160–1170.
140 Y. Zhu, Y. Yang, Y. Wang, B. Yao, X. Lin, B. Zhang, H. Zhan, Z. Xie and Y. Cheng, *Adv. Opt. Mater.*, 2018, **6**, 1701320.
141 Y. Wang, Y. Zhu, X. Lin, Y. Yang, B. Zhang, H. Zhan, Z. Xie and Y. Cheng, *J. Mater. Chem. C*, 2018, **6**, 568–574.
142 J. Hu, Q. Li, X. Wang, S. Shao, L. Wang, X. Jing and F. Wang, *Angew. Chem., Int. Ed.*, 2019, **58**, 8405–8409.
143 Q. Li, J. Hu, J. Lv, X. Wang, S. Shao, L. Wang, X. Jing and F. Wang, *Angew. Chem., Int. Ed.*, 2020, **59**, 20174–20182.
144 X. L. Chen, J. H. Jia, R. Yu, J. Z. Liao, M. X. Yang and C. Z. Lu, *Angew. Chem., Int. Ed.*, 2017, **56**, 15006–15009.
145 X. Tang, Y. Tao, H. Liu, F. Liu, X. He, Q. Peng, J. Li and P. Lu, *Front. Chem.*, 2019, **7**, 373.
146 I. S. Park, K. Matsuo, N. Aizawa and T. Yasuda, *Adv. Funct. Mater.*, 2018, **28**, 1802031.
147 K. Matsuo and T. Yasuda, *Chem. Sci.*, 2019, **10**, 10687–10697.
148 G. Xia, C. Qu, Y. Zhu, J. Ye, K. Ye, Z. Zhang and Y. Wang, *Angew. Chem., Int. Ed.*, 2021, **60**, 9598–9603.
149 G. Meng, X. Chen, X. Wang, N. Wang, T. Peng and S. Wang, *Adv. Opt. Mater.*, 2019, **7**, 1900130.
150 H. J. Kim, M. Godumala, S. K. Kim, J. Yoon, C. Y. Kim, H. Park, J. H. Kwon, M. J. Cho and D. H. Choi, *Adv. Opt. Mater.*, 2020, **8**, 1902175.
151 H. J. Kim, H. Kang, J. E. Jeong, S. H. Park, C. W. Koh, C. W. Kim, H. Y. Woo, M. J. Cho, S. Park and D. H. Choi, *Adv. Funct. Mater.*, 2021, **31**, 2102588.
152 F. Chen, J. Hu, X. Wang, S. Shao, L. Wang, X. Jing and F. Wang, *Sci. China: Chem.*, 2020, **63**, 1112–1120.
153 R. Furue, T. Nishimoto, I. S. Park, J. Lee and T. Yasuda, *Angew. Chem., Int. Ed.*, 2016, **55**, 7171–7175.

© 2022 The Author(s). Published by the Royal Society of Chemistry